

Higgs Precision (Higgcision) Era begins

Kingman Cheung^{1,2}, Jae Sik Lee³, and Po-Yan Tseng¹

¹ *Department of Physics, National Tsing Hua University, Hsinchu 300, Taiwan*

² *Division of Quantum Phases and Devices, School of Physics,
Konkuk University, Seoul 143-701, Republic of Korea*

³ *Department of Physics, Chonnam National University,
300 Yongbong-dong, Buk-gu, Gwangju, 500-757, Republic of Korea*

(Dated: October 29, 2018)

Abstract

After the discovery of the Higgs boson at the LHC, it is natural to start the research program on the precision study of the Higgs-boson couplings to various standard model (SM) particles. We provide a generic framework for the deviations of the couplings from their SM values by introducing a number of parameters. We show that a large number of models beyond the SM can be covered, including two-Higgs-doublet models, supersymmetric models, little-Higgs models, extended Higgs sectors with singlets, and fourth generation models. We perform global fits to the most updated data from CMS, ATLAS, and Tevatron under various initial conditions of the parameter set. In particular, we have made explicit comparisons between the fitting results *before* and *after* the Moriond 2013 meetings. Highlights of the results include: (i) the nonstandard decay branching ratio of the Higgs boson is less than 22%; (ii) the most efficient way to achieve the best fit for the data before the Moriond update is to introduce additional particle contributions to the triangular-loop functions of $H\gamma\gamma$ and Hgg vertices; (iii) the 1σ allowed range of the relative coupling of HVV is $1.01^{+0.13}_{-0.14}$, which means that the electroweak-symmetry breaking contribution from the observed Higgs boson leaves only a small room for other Higgs bosons; (iv) the current data do not rule out pseudoscalar couplings nor pseudoscalar contributions to the $H\gamma\gamma$ and Hgg vertices; and (v) the SM Higgs boson provides the best fit to all the current Higgs data.

I. INTRODUCTION

It is of very high expectation that the observed particle at the Large Hadron Collider (LHC) [1, 2] is the long-sought Higgs boson of the standard model (SM), which was proposed in 1960s [3]. At the end of 2011, both the ATLAS and CMS [4] experiments at the LHC have seen some excess of events of a possible Higgs boson candidate in the decay modes of $H \rightarrow \gamma\gamma$, $H \rightarrow WW^* \rightarrow \ell^+\nu\ell^-\bar{\nu}$, and $H \rightarrow ZZ^* \rightarrow 4\ell$ channels. Finally, the discovery was announced in July 2012 by ATLAS [1] and CMS [2]. The channels WW and ZZ are consistent with the predictions of the SM Higgs boson, while the $\gamma\gamma$ rate is somewhat higher than expectation. Some evidence is seen in the $b\bar{b}$ mode at the Tevatron [5], but the mass range is quite wide. On the other hand, the $\tau^+\tau^-$ mode appears to be suppressed before the very recent update, although the data contain large uncertainties.

A previous update was presented at the *Hadron Collider Physics Symposium 2012* [6, 7] and in a series of experimental notes [8–15] at the end of 2012. At that time, the $\tau^+\tau^-$ data began to appear, but still too early to say something concrete. The diphoton production rate was somewhat higher than the SM prediction by a factor of 1.4 – 1.8. Nevertheless, the deviations are only 1 – 2 σ . A large number of models have been put forward to account for the observed particle at 125 GeV, including the SM, supersymmetric models such as the minimal supersymmetric standard model [16], the next-to-minimal supersymmetric standard model [17], the $U(1)$ -extended minimal supersymmetric standard model [18], fermiophobic Higgs boson [19], two-Higgs-doublet models (2HDM) of various types [20], Randall-Sundrum radion [21], inert-Higgs doublet model [22], etc (a summary of various models can be found in Ref. [23].) They all can explain the enhanced diphoton rate with some choices of parameter space. Yet, more data are needed in order to firmly establish the excess in the diphoton channel. The most recent update was during the Moriond 2013 meetings [24]. The updated data can be found in a number of conference note from the ATLAS [25, 26] and CMS [27–30].

Currently, a number of decay and production channels are available. On the production side, there are gluon fusion (ggF), vector-boson fusion (VBF), and associated production with a $V = W/Z$ boson (VH) and top quarks (ttH); while the decay channels include $\gamma\gamma$, $ZZ^* \rightarrow 4\ell$, $WW^* \rightarrow \ell^+\nu\ell^-\bar{\nu}$, $b\bar{b}$, and $\tau^+\tau^-$. One can extract useful information on the size of the Higgs boson couplings from the available data. However, in order to do that the dependence of various production and decay modes on the Higgs couplings has to be

taken into account correctly. For example, the ggF depends on the Higgs couplings to a pair of top ($H\bar{t}t$) and bottom ($H\bar{b}b$) quarks, as well as possible existence of exotic colored particles running in the loop; while the VBF and VH depend only on the Higgs coupling to a pair of vector bosons (HVV). Also, the decays into WW^* and ZZ^* simply depend on HVV , and the decays into $b\bar{b}$ and $\tau^+\tau^-$ depend on $H\bar{b}b$ and $H\bar{\tau}\tau$ respectively; but the decay into $\gamma\gamma$ involves all of the above couplings and perhaps new electrically-charged particles in the triangular loop. A global analysis of all the Higgs couplings using all the available data would be extremely useful to identify the observed Higgs boson. Once we disentangle each of the Higgs couplings from the global data set, we can use the result to compare with models. This approach is in contrast to those top-down approaches, which usually start with a model, calculate the signal strengths, and then find the allowed parameter space to fit to the data.

Indeed, the Higgs precision era just begins. There have been a number of works in the past few months going in this direction, in a more or less model-independent framework [31–51], in 2HDM framework [52–59], and in supersymmetry [60–64]. Also, there are studies toward the determination of the spin-parity nature of the Higgs boson (see Ref. [65] for more references in literature) that cannot be obtained from the signal strengths.

About a couple of weeks after we posted the first version of our paper to arXiv, both ATLAS and CMS Collaborations have updated their Higgs data during the Moriond 2013 meetings [24]. They have released a series of conference notes [26–30] on the new data. In particular, the most striking is the change of the diphoton data by the CMS [27]. Because of this change the overall fits also change dramatically. In the following, we will show the results *before* and *after* the Moriond 2013 meetings.

The characteristic features of our analysis are summarized as follows.

1. We allow the Yukawa couplings to the charged-lepton ($H\bar{\tau}\tau$) and the down-quark ($H\bar{b}b$) sectors to vary independently. This can be realized in some versions of the 2HDM. This has also been adopted in a few previous works.
2. We allow an independent deviation in the total decay width of the Higgs boson, in addition to the parameters of the Yukawa and HVV couplings. This can be realized in nonstandard decays of the Higgs boson, e.g., $h \rightarrow \tilde{\chi}_1^0 \tilde{\chi}_1^0$ in SUSY models, $H \rightarrow aa$ where a stands for some lighter Higgs bosons in the model. This has been included in

some previous works. An interesting result is obtained because of this improvement. The nonstandard decay width is constrained to be less than 1.2 MeV at 95% CL, which accounts for a branching ratio of about 22%.

3. In the loop vertices of $H\gamma\gamma$ and Hgg , we allow new parameters ΔS^γ and ΔS^g respectively, which can most conveniently account for the effects of new particles contributing to the loops.
4. Preliminarily, the pseudoscalar interpretation of the observed Higgs boson is disfavored. However, it may not apply to the case of CP-mixed state carrying both scalar-type and pseudoscalar-type couplings simultaneously. We perform a whole new analysis including both scalar-type and pseudoscalar-type Yukawa couplings, and both radiatively-induced scalar and pseudoscalar $H\gamma\gamma$ and Hgg vertices. We show that pseudoscalar couplings are actually not ruled out based on signal strengths only, by giving equivalently good fits compared to the CP-conserving case.

The organization of the paper is as follows. In the next section, we describe the interactions of the Higgs boson, including deviations in the Yukawa couplings and deviations in the loop functions of $H\gamma\gamma$, Hgg , and $HZ\gamma$ vertices, as well as the notation used in the analysis. In Sec. III, we list the Higgs boson data both *before* and *after* Moriond 2013 meetings that we use in this analysis. We present the results of various fits in Sec. IV, and the readers can see how the fits change when the Higgs data are changed. In Sec. V, we present the results using both scalar-type and pseudoscalar-type couplings. We conclude in Sec. VI.

II. FORMALISM

A. Higgs Couplings

We follow the conventions and notations of CPsuperH [66–68] for the Higgs couplings to the SM particles assuming the Higgs boson is a generally CP-mixed state without carrying any definite CP-parity.

- Higgs couplings to fermions:

$$\mathcal{L}_{H\bar{f}f} = - \sum_{f=u,d,l} \frac{gm_f}{2M_W} \sum_{i=1}^3 H \bar{f} \left(g_{H\bar{f}f}^S + ig_{H\bar{f}f}^P \gamma_5 \right) f . \quad (1)$$

For the SM couplings, $g_{H\bar{f}f}^S = 1$ and $g_{H\bar{f}f}^P = 0$.

- Higgs couplings to the massive vector bosons:

$$\mathcal{L}_{HVV} = g M_W \left(g_{HWW} W_\mu^+ W^{-\mu} + g_{HZZ} \frac{1}{2c_W^2} Z_\mu Z^\mu \right) H. \quad (2)$$

For the SM couplings, we have $g_{HWW} = g_{HZZ} \equiv g_{HVV} = 1$, respecting the custodial symmetry.

- Higgs couplings to two photons: The amplitude for the decay process $H \rightarrow \gamma\gamma$ can be written as

$$\mathcal{M}_{\gamma\gamma H} = -\frac{\alpha M_H^2}{4\pi v} \left\{ S^\gamma(M_H) (\epsilon_{1\perp}^* \cdot \epsilon_{2\perp}^*) - P^\gamma(M_H) \frac{2}{M_H^2} \langle \epsilon_1^* \epsilon_2^* k_1 k_2 \rangle \right\}, \quad (3)$$

where $k_{1,2}$ are the momenta of the two photons and $\epsilon_{1,2}$ the wave vectors of the corresponding photons, $\epsilon_{1\perp}^\mu = \epsilon_1^\mu - 2k_1^\mu(k_2 \cdot \epsilon_1)/M_H^2$, $\epsilon_{2\perp}^\mu = \epsilon_2^\mu - 2k_2^\mu(k_1 \cdot \epsilon_2)/M_H^2$ and $\langle \epsilon_1 \epsilon_2 k_1 k_2 \rangle \equiv \epsilon_{\mu\nu\rho\sigma} \epsilon_1^\mu \epsilon_2^\nu k_1^\rho k_2^\sigma$. The decay rate of $H \rightarrow \gamma\gamma$ is proportional to $|S^\gamma|^2 + |P^\gamma|^2$. Including some additional loop contributions from new particles, the scalar and pseudoscalar form factors, retaining only the dominant loop contributions from the third-generation fermions and W^\pm , are given by ¹

$$\begin{aligned} S^\gamma(M_H) &= 2 \sum_{f=b,t,\tau} N_C Q_f^2 g_{H\bar{f}f}^S F_{sf}(\tau_f) - g_{HWW} F_1(\tau_W) + \Delta S^\gamma, \\ P^\gamma(M_H) &= 2 \sum_{f=b,t,\tau} N_C Q_f^2 g_{H\bar{f}f}^P F_{pf}(\tau_f) + \Delta P^\gamma, \end{aligned} \quad (4)$$

where $\tau_x = M_H^2/4m_x^2$, $N_C = 3$ for quarks and $N_C = 1$ for taus, respectively. The additional contributions ΔS^γ and ΔP^γ are assumed to be real in our work, as there are unlikely any new *charged* particles lighter than $M_H/2$.

Taking $M_H = 125.5$ GeV, we find that

$$\begin{aligned} S^\gamma &\simeq -8.35 g_{HWW} + 1.76 g_{H\bar{t}t}^S + (-0.015 + 0.017 i) g_{H\bar{b}b}^S \\ &\quad + (-0.024 + 0.021 i) g_{H\bar{\tau}\tau}^S + (-0.007 + 0.005 i) g_{H\bar{c}c}^S + \Delta S^\gamma \\ P^\gamma &\simeq 2.78 g_{H\bar{t}t}^P + (-0.018 + 0.018 i) g_{H\bar{b}b}^P \\ &\quad + (-0.025 + 0.022 i) g_{H\bar{\tau}\tau}^P + (-0.007 + 0.005 i) g_{H\bar{c}c}^P + \Delta P^\gamma \end{aligned} \quad (5)$$

giving $S_{\text{SM}}^\gamma = -6.64 + 0.043 i$ and $P_{\text{SM}}^\gamma = 0$.

¹ For the loop functions of $F_{sf,pf,1}(\tau)$, we refer to, for example, Ref. [66].

- Higgs couplings to two gluons: Similar to $H \rightarrow \gamma\gamma$, the amplitude for the decay process $H \rightarrow gg$ can be written as

$$\mathcal{M}_{ggH} = -\frac{\alpha_s M_H^2 \delta^{ab}}{4\pi v} \left\{ S^g(M_H) (\epsilon_{1\perp}^* \cdot \epsilon_{2\perp}^*) - P^g(M_H) \frac{2}{M_H^2} \langle \epsilon_1^* \epsilon_2^* k_1 k_2 \rangle \right\}, \quad (6)$$

where a and b ($a, b = 1$ to 8) are indices of the eight $SU(3)$ generators in the adjoint representation. The decay rate of $H \rightarrow gg$ is proportional to $|S^g|^2 + |P^g|^2$. Again, including some additional loop contributions from new particles, the scalar and pseudoscalar form factors are given by

$$\begin{aligned} S^g(M_H) &= \sum_{f=b,t} g_{H\bar{f}f}^S F_{sf}(\tau_f) + \Delta S^g, \\ P^g(M_H) &= \sum_{f=b,t} g_{H\bar{f}f}^P F_{pf}(\tau_f) + \Delta P^g. \end{aligned} \quad (7)$$

The additional contributions ΔS^g and ΔP^g are assumed to be real again.

Taking $M_H = 125.5$ GeV, we find that

$$\begin{aligned} S^g &\simeq 0.688 g_{H\bar{t}t}^S + (-0.037 + 0.050 i) g_{H\bar{b}b}^S + \Delta S^g, \\ P^g &\simeq 1.047 g_{H\bar{t}t}^P + (-0.042 + 0.050 i) g_{H\bar{b}b}^P + \Delta P^g, \end{aligned} \quad (8)$$

giving $S_{\text{SM}}^g = 0.651 + 0.050 i$ and $P_{\text{SM}}^g = 0$.

- Higgs couplings to Z and γ : The amplitude for the decay process $H \rightarrow Z(k_1, \epsilon_1) \gamma(k_2, \epsilon_2)$ can be written as

$$\mathcal{M}_{Z\gamma H} = -\frac{\alpha}{2\pi v} \left\{ S^{Z\gamma}(M_H) [k_1 \cdot k_2 \epsilon_1^* \cdot \epsilon_2^* - k_1 \cdot \epsilon_2^* k_2 \cdot \epsilon_1^*] - P^{Z\gamma}(M_H) \langle \epsilon_1^* \epsilon_2^* k_1 k_2 \rangle \right\} \quad (9)$$

where $k_{1,2}$ are the momenta of the Z boson and the photon (we note that $2k_1 \cdot k_2 = M_H^2 - M_Z^2$), $\epsilon_{1,2}$ are their polarization vectors. The scalar and pseudoscalar form factors are given by

$$\begin{aligned} S^{Z\gamma}(M_H) &= 2 \sum_{f=t,b,\tau} Q_f N_C^f m_f^2 \frac{I_3^f - 2s_W^2 Q_f}{s_W c_W} g_{H\bar{f}f}^S F_f^{(0)} + M_Z^2 \cot \theta_W g_{HWW} F_W + \Delta S^{Z\gamma}, \\ P^{Z\gamma}(M_H) &= 2 \sum_{f=t,b,\tau} Q_f N_C^f m_f^2 \frac{I_3^f - 2s_W^2 Q_f}{s_W c_W} g_{H\bar{f}f}^P F_f^{(5)} + \Delta P^{Z\gamma}. \end{aligned} \quad (10)$$

The additional contributions $\Delta S^{Z\gamma}$ and $\Delta P^{Z\gamma}$ are assumed to be real. The loop functions are ²

$$\begin{aligned} F_f^{(0)} &= C_0(m_f^2) + 4C_2(m_f^2), \\ F_f^{(5)} &= C_0(m_f^2), \\ F_W &= 2 \left[\frac{M_H^2}{M_W^2} (1 - 2c_W^2) + 2(1 - 6c_W^2) \right] C_2(M_W^2) + 4(1 - 4c_W^2) C_0(M_W^2). \end{aligned} \quad (11)$$

Taking $M_H = 125.5$ GeV, we find

$$\begin{aligned} S^{Z\gamma} &\simeq -11.966 g_{HWW} + 0.615 g_{H\bar{t}t}^S + (-0.008 + 0.004 i) g_{H\bar{b}b}^S \\ &\quad + (-0.0004 + 0.0002 i) g_{H\bar{\tau}\tau}^S + \Delta S^{Z\gamma}, \\ P^{Z\gamma} &\simeq 0.933 g_{H\bar{t}t}^P + (-0.009 + 0.004 i) g_{H\bar{b}b}^P \\ &\quad + (-0.0004 + 0.0002 i) g_{H\bar{\tau}\tau}^S + \Delta P^{Z\gamma}, \end{aligned} \quad (12)$$

giving $S_{\text{SM}}^{Z\gamma} = -11.358 + 0.004 i$ and $P_{\text{SM}}^{Z\gamma} = 0$.

In passing, we recall that the Z -boson couplings to the quarks and leptons are given by

$$\mathcal{L}_{Z\bar{f}f} = -g_Z \bar{f} \gamma^\mu (v_{Z\bar{f}f} - a_{Z\bar{f}f} \gamma_5) f Z_\mu, \quad (13)$$

where $g_Z = e/(s_W c_W)$, $v_{Z\bar{f}f} = I_3^f/2 - Q_f s_W^2$ and $a_{Z\bar{f}f} = I_3^f/2$ with $I_3^u = 1/2$ and $I_3^{d,l} = -1/2$.

Finally, we define the ratios of the effective Higgs couplings to gg , $\gamma\gamma$, and $Z\gamma$ relative to the SM ones as follows:

$$C_g \equiv \sqrt{\frac{|S^g|^2 + |P^g|^2}{|S_{\text{SM}}^g|^2}}; \quad C_\gamma \equiv \sqrt{\frac{|S^\gamma|^2 + |P^\gamma|^2}{|S_{\text{SM}}^\gamma|^2}}; \quad C_{Z\gamma} \equiv \sqrt{\frac{|S^{Z\gamma}|^2 + |P^{Z\gamma}|^2}{|S_{\text{SM}}^{Z\gamma}|^2}}. \quad (14)$$

Note that the ratios of decay rates relative to the SM are given by $|C_g|^2$, $|C_\gamma|^2$, and $|C_{Z\gamma}|^2$, respectively.

² For the functions of $C_{0,2}(m^2)$, we refer to [69].

B. Signal strengths

The theoretical signal strength may be written as the product

$$\hat{\mu}(\mathcal{P}, \mathcal{D}) \simeq \hat{\mu}(\mathcal{P}) \hat{\mu}(\mathcal{D}) \quad (15)$$

where $\mathcal{P} = \text{ggF}, \text{VBF}, \text{VH}, \text{ttH}$ denote the production mechanisms and $\mathcal{D} = \gamma\gamma, ZZ, WW, b\bar{b}, \tau\bar{\tau}$ the decay channels. More explicitly, we are taking

$$\begin{aligned} \hat{\mu}(\text{ggF}) &= \frac{|S^g(M_H)|^2 + |P^g(M_H)|^2}{|S_{\text{SM}}^g(M_H)|^2}, \\ \hat{\mu}(\text{VBF}) &= g_{HWW, HZZ}^2, \\ \hat{\mu}(\text{VH}) &= g_{HWW, HZZ}^2, \\ \hat{\mu}(\text{ttH}) &= (g_{H\bar{t}t}^S)^2 + (g_{H\bar{t}t}^P)^2; \end{aligned} \quad (16)$$

and

$$\hat{\mu}(\mathcal{D}) = \frac{B(H \rightarrow \mathcal{D})}{B(H_{\text{SM}} \rightarrow \mathcal{D})} \quad (17)$$

with

$$B(H \rightarrow \mathcal{D}) = \frac{\Gamma(H \rightarrow \mathcal{D})}{\Gamma_{\text{tot}}(H) + \Delta\Gamma_{\text{tot}}} \quad (18)$$

Note that we introduce an arbitrary non-SM contribution $\Delta\Gamma_{\text{tot}}$ to the total decay width. Incidentally, $\Gamma_{\text{tot}}(H)$ becomes the SM total decay width when $g_{H\bar{f}f}^S = 1$, $g_{H\bar{f}f}^P = 0$, $g_{HWW, HZZ} = 1$, $\Delta S^{\gamma, g, Z\gamma} = \Delta P^{\gamma, g, Z\gamma} = 0$.

The experimentally observed signal strength should be compared to the theoretical one summed over all production mechanisms:

$$\mu(\mathcal{Q}, \mathcal{D}) = \sum_{\mathcal{P}=\text{ggF}, \text{VBF}, \text{VH}, \text{ttH}} C_{\mathcal{Q}\mathcal{P}} \hat{\mu}(\mathcal{P}, \mathcal{D}) \quad (19)$$

where \mathcal{Q} denote the experimentally defined channel involved with the decay \mathcal{D} and the decomposition coefficients $C_{\mathcal{Q}\mathcal{P}}$ may depend on the relative Higgs production cross sections for a given Higgs-boson mass, experimental cuts, etc.

The χ^2 associated with an uncorrelated observable is

$$\chi^2(\mathcal{Q}, \mathcal{D}) = \frac{[\mu(\mathcal{Q}, \mathcal{D}) - \mu^{\text{EXP}}(\mathcal{Q}, \mathcal{D})]^2}{[\sigma^{\text{EXP}}(\mathcal{Q}, \mathcal{D})]^2}, \quad (20)$$

where $\sigma^{\text{EXP}}(\mathcal{Q}, \mathcal{D})$ denotes the experimental error. For two correlated observables, we use

$$\chi^2(\mathcal{Q}_1, \mathcal{D}; \mathcal{Q}_2, \mathcal{D}) = \left\{ \frac{[\mu(\mathcal{Q}_1, \mathcal{D}) - \mu^{\text{EXP}}(\mathcal{Q}_1, \mathcal{D})]^2}{[\sigma^{\text{EXP}}(\mathcal{Q}_1, \mathcal{D})]^2} + \frac{[\mu(\mathcal{Q}_2, \mathcal{D}) - \mu^{\text{EXP}}(\mathcal{Q}_2, \mathcal{D})]^2}{[\sigma^{\text{EXP}}(\mathcal{Q}_2, \mathcal{D})]^2} - 2\rho \frac{[\mu(\mathcal{Q}_1, \mathcal{D}) - \mu^{\text{EXP}}(\mathcal{Q}_1, \mathcal{D})][\mu(\mathcal{Q}_2, \mathcal{D}) - \mu^{\text{EXP}}(\mathcal{Q}_2, \mathcal{D})]}{[\sigma^{\text{EXP}}(\mathcal{Q}_1, \mathcal{D})][\sigma^{\text{EXP}}(\mathcal{Q}_2, \mathcal{D})]} \right\} / (1 - \rho^2) \quad (21)$$

where ρ is the correlation coefficient.

C. Parameters using in the fits

Without loss of generality we use the following notation for the parameters in the fits:

$$\begin{aligned} C_u^S &= g_{H\bar{u}u}^S, & C_d^S &= g_{H\bar{d}d}^S, & C_\ell^S &= g_{H\bar{\ell}\ell}^S; & C_v &= g_{HVV}; \\ C_u^P &= g_{H\bar{u}u}^P, & C_d^P &= g_{H\bar{d}d}^P, & C_\ell^P &= g_{H\bar{\ell}\ell}^P. \end{aligned} \quad (22)$$

Here we assume generation independence and also custodial symmetry between the W and Z bosons. Note that the tree-level pseudoscalar couplings to W and Z bosons are zero. The first and second generation fermion couplings to the Higgs boson is rather small, but if in the near future the $H \rightarrow \mu^+\mu^-$ can be measured, one may set independent parameters C_μ and C_τ (for the present work we consider them to be the same.)

In the fits, we further use

$$\Delta S^g, \quad \Delta S^\gamma; \quad \Delta P^g, \quad \Delta P^\gamma \quad (23)$$

which are real quantities assuming that any new particles running in the triangular loop are heavier than one half of the Higgs boson mass. Note that the quantities S^g and S^γ are in general complex in both the SM and beyond the SM. For the most direct comparison with experimental data we use C_γ and C_g in the plots.³

Another important quantity is the additional contributions to the width of the Higgs boson, $\Delta\Gamma_{\text{tot}}$ as in Eq. (18). The parameter $\Delta\Gamma_{\text{tot}}$ takes into account the nonstandard decays of the Higgs boson, e.g., $h_1 \rightarrow a_1 a_1$ in NMSSM, $h_1 \rightarrow \tilde{\chi}_1^0 \tilde{\chi}_1^0$ in SUSY, $h_2 \rightarrow h_1 h_1$ in

³ The quantities ΔC_γ and ΔC_g defined in Ref. [47] are in general complex. It would be more difficult to use them as fitting parameters.

other extended Higgs models. The current data still allow a small amount of Higgs invisible decay branching ratio.

We first use the following scalar-type couplings:

$$C_u^S, C_d^S, C_\ell^S, C_v, \Delta S^g, \Delta S^\gamma, \Delta\Gamma_{\text{tot}}$$

to fit to the Higgs data in Sec. IV, where we focus on the SM-like Higgs boson. In Sec. V, where we also consider the possibility that the observed Higgs boson can allow some level of pseudoscalar-type couplings

$$C_u^P, C_d^P, C_\ell^P, \Delta P^\gamma, \Delta P^g,$$

in addition to the scalar ones.

D. Two-Higgs Doublet Models

Two-Higgs-doublet models employ two Higgs doublets in the process of electroweak-symmetry breaking (EWSB). A discrete Z_2 symmetry is usually imposed in order to avoid dangerous tree-level flavor-changing neutral currents. The most studied are the type I and type II models. They can easily be covered by the framework presented in this paper. We illustrate using the model II.

The Higgs sector consists of two Higgs doublets $H_u = (H_u^+ H_u^0)^T$ and $H_d = (H_d^+ H_d^0)^T$ where the subscripts u, d denote the right-handed quark singlet fields that the Higgs doublets couple to. After EWSB, there are two CP-even, one CP-odd, and a pair of charged Higgs bosons. The parameters of the model in the CP-conserving case can be chosen as

$$m_h, m_H, m_A, m_{H^\pm}, \tan\beta \equiv \frac{v_u}{v_d}, \alpha$$

where α is the mixing angle between the two CP-even Higgs bosons. The couplings of the lighter CP-even Higgs boson h (assumed to be the observed boson) to the tau, bottom, top quarks, and W/Z boson relative to their corresponding SM values are given by

$$\begin{array}{cccc}
\tau^- \tau^+ & b\bar{b} & t\bar{t} & W^+ W^- / ZZ \\
h: & -\sin\alpha / \cos\beta & -\sin\alpha / \cos\beta & \cos\alpha / \sin\beta \quad \sin(\beta - \alpha)
\end{array}$$

Therefore, we can equate these quantities with the definitions of $C_u^S, C_d^S, C_\ell^S, C_v$, given by

$$C_u^S = \frac{\cos\alpha}{\sin\beta}, \quad C_d^S = C_\ell^S = -\frac{\sin\alpha}{\cos\beta}, \quad C_v = \sin(\beta - \alpha). \quad (24)$$

From the above relations, one may derive the following consistency relations which should hold in the type II model:

$$\begin{aligned}\cos^2 \beta &= \frac{C_v - C_u^S}{C_{d,\ell}^S - C_u^S}, & \sin^2 \beta &= \frac{C_{d,\ell}^S - C_v}{C_{d,\ell}^S - C_u^S}; \\ \sin^2 \alpha &= \frac{C_v - 1/C_u^S}{1/C_{d,\ell}^S - 1/C_u^S}, & \cos^2 \alpha &= \frac{1/C_{d,\ell}^S - C_v}{1/C_{d,\ell}^S - 1/C_u^S}.\end{aligned}\tag{25}$$

On the other hand, the only additional particle that can run in the triangular loop of $h\gamma\gamma$ is the charged Higgs boson. Also, there are no new particles other than the SM particles that the Higgs boson h can decay into. Therefore, the other quantities

$$\Delta S^\gamma \neq 0, \quad \Delta S^g = 0, \quad \Delta \Gamma_{\text{tot}} = 0.\tag{26}$$

Thus, the two-Higgs doublet models, in general, can be covered by our framework.

In more complicated Higgs sectors, e.g., with additional singlets, there may be lighter Higgs bosons that the observed Higgs boson can decay into. In such a case, the additional decay modes will contribute to $\Delta \Gamma_{\text{tot}}$.

E. Models with singlet Higgs bosons

Simple extensions of the SM Higgs sector with one or more Higgs singlet fields are attractive, because they can often provide a dark matter candidate once some kinds of discrete symmetries are imposed on the extra fields. Some variants can be found in Refs. [70–73]. In the simplest version [73], the Higgs sector consists of the usual SM Higgs doublet Φ and a real singlet Higgs field χ . They couple to each other via a renormalizable interaction $\rho\chi^2\Phi^\dagger\Phi$. A discrete Z_2 symmetry is imposed on $\chi \rightarrow -\chi$ such that χ cannot develop the vacuum expectation value (VEV) and becomes a dark matter candidate. After Φ develops the VEV, χ couples to the H via the interactions $\chi^2 H$ and $\chi^2 H^2$. Therefore, the Higgs boson, in addition to the couplings to the SM fermions, also couples to a pair of χ s. The only modification in our framework is the total decay width, accommodated by $\Delta \Gamma_{\text{tot}}$.

F. Supersymmetric models

There are many varieties in supersymmetric models which contain at least two Higgs doublets. In the minimal supersymmetric extension of the SM (MSSM), there are three

neutral Higgs states and, in principle, any of them can be the candidate for the observed particle at 125 GeV. If the i -th ($i = 1, 2, 3$) Higgs state is assumed to be the observed particle, we have

$$C_u^S = \frac{O_{\phi_2 i}}{\sin \beta}, \quad C_d^S = C_\ell^S = \frac{O_{\phi_1 i}}{\cos \beta}, \quad C_v = O_{\phi_1 i} \cos \beta + O_{\phi_2 i} \sin \beta;$$

$$C_u^P = -\frac{\cos \beta}{\sin \beta} O_{ai}, \quad C_d^P = C_\ell^P = -\frac{\sin \beta}{\cos \beta} O_{ai}, \quad (27)$$

where $O_{\phi_1 i, \phi_2 i}$ and O_{ai} denote the CP-even and CP-odd components of the i -th Higgs state, respectively ⁴, and $\cos \beta$ and $\sin \beta$ are defined in the same way as in the type-II 2HDM. Including the threshold corrections to the third-generation Yukawa couplings, the above tree-level relations undergo some changes. Nevertheless, this case can be covered because we are treating $C_d^{S,P}$ and $C_\ell^{S,P}$ independently in our framework.

Beyond the MSSM there could be more than three neutral Higgs states. In this case, it is straightforward to find similar relations as in Eq. (27). For example, in the next-to-minimal supersymmetric standard model (NMSSM) the neutral Higgs bosons have a 5×5 mixing matrix [74].

Any bosonic and fermionic contributions of SUSY particles to the $H\gamma\gamma$ and Hgg vertices, including the charged Higgs-boson contribution, can be nicely accommodated by using the parameters $\Delta S^{g,\gamma}$ and $\Delta P^{g,\gamma}$. Also, the parameter $\Delta\Gamma_{\text{tot}}$ can take into account any Higgs decays into the non-SM particles.

G. Little Higgs models

Little Higgs models belong to a class of models in which the quadratic divergences to the Higgs boson are cancelled by a set of particles having the same spin statistics as the SM particles. For each SM particle there corresponds a little-Higgs (LH) partner with the coupling to the Higgs boson specifically designed in such a way that the quadratic divergence is cancelled. For example, the W boson has the LH partner W_H . A phenomenological interesting example is the littlest Higgs model [75], the phenomenology of which was described in details in Ref. [76].

In general, the Yukawa couplings of the SM-like Higgs boson could be different from the SM, depending on the gauge structure of the LH model; so are the couplings to the W/Z

⁴ For the precise definition of the orthogonal 3×3 Higgs-boson-mixing matrix O , we refer to Ref. [66].

bosons. Other heavy LH partners, if they are electrically charged, can run in the triangular loop of $H\gamma\gamma$ vertex, and if they carry color they will contribute to Hgg vertex. If there are other light Higgs bosons that the SM-like Higgs boson can decay into, they will increase the decay width Γ_{tot} . Thus, the LH models can be accommodated in the present framework by $C_{u,d,\ell}^{S,P}$, C_v , ΔS^γ , ΔS^g , and $\Delta\Gamma_{\text{tot}}$.

Recent analyses of little Higgs models with respect to current Higgs data can be found in Refs. [77, 78].

H. Fourth Generation model

The sequential fourth generation model is a simple extension of the SM by adding an analogous repetition of a generation of fermions. The new charged leptons and quarks can run in the loop of $H\gamma\gamma$ while the colored quarks run in the loop of Hgg . Thus, the fourth generation contributes to ΔS^γ and ΔS^g only while all the Yukawa couplings are the same as the SM and $\Delta\Gamma_{\text{tot}} = 0$.

III. HIGGS DATA

Current Higgs data focus on a few decay channels of the Higgs boson: (i) $h \rightarrow \gamma\gamma$, (ii) $h \rightarrow ZZ^* \rightarrow \ell^+\ell^-\ell^+\ell^-$, (iii) $h \rightarrow WW^* \rightarrow \ell^+\bar{\nu}\ell^-\nu$, (iv) $h \rightarrow b\bar{b}$, and (v) $h \rightarrow \tau^+\tau^-$. Within each decay mode both CMS and ATLAS have reported a number of channels, such as inclusive, vector-boson-fusion tagged, and/or VH tagged. All the available ATLAS, CMS, and Tevatron data in these five decay channels are shown in Tables I–V, respectively. Both sets of data *before* and *after* the Moriond 2013 meetings are listed in the tables. We have used 22 data points in our analysis. The chi-square of all these 22 data points relative to the SM is about 17.5 and 18.94 for the data set *before* and *after* Moriond, respectively, and so the chi-square per degree of freedom (dof) is about $17.5/22 = 0.80$ and $18.94/22 = 0.86$, which means that the SM is a reasonably good fit to the Higgs data. The goodness of the fit, measured by the p -value, is about $p = 0.74$ and $p = 0.65$ for the data *before* and *after* Moriond, respectively.⁵

⁵ Assuming the goodness-of-fit statistics follows a χ^2 probability density function, the p -value for the hypothesis is given by [79]

$$p = \int_{\chi^2}^{\infty} f(z; n) dz$$

13

There are four production modes: gluon fusion (ggF), vector-boson fusion (VBF), associated production with a W/Z boson (VH), and associated production with a $t\bar{t}$ pair (ttH). The production cross sections for each production modes at the LHC could be found in Ref.[80]. For $\sqrt{s} = 7$ TeV and Higgs-boson mass $M_H = 126$ GeV, the cross sections are:

$$\sigma(\text{ggF}) = 15.080, \sigma(\text{VBF}) = 1.211, \sigma(\text{VH}) = 0.8653, \sigma(\text{ttH}) = 0.0843 \text{ pb}, \quad (28)$$

where $\sigma(\text{VH}) = \sigma(WH) + \sigma(ZH)$. For $\sqrt{s} = 8$ TeV and Higgs-boson mass $M_H = 126$ GeV the cross sections are:

$$\sigma(\text{ggF}) = 19.220, \sigma(\text{VBF}) = 1.568, \sigma(\text{VH}) = 1.0625, \sigma(\text{ttH}) = 0.1271 \text{ pb}. \quad (29)$$

Since the ATLAS and CMS from the above tables combined both $\sqrt{s} = 7$ TeV and $\sqrt{s} = 8$ TeV, we take the luminosities for the 7 and 8 TeV data as weights to recalculate the cross section of each production mode. Take the VH mode of “untagged” channel of “CMS (5.1 fb⁻¹ at 7 TeV + 19.6 fb⁻¹ at 8 TeV)” (after Moriond 2013) from Table I as an example, the weighted cross section of the VH mode is

$$\sigma(\text{VH})_{\text{weighted}} = \frac{5.1 \text{ fb}^{-1} \times 0.8653 \text{ pb} + 19.6 \text{ fb}^{-1} \times 1.0625 \text{ pb}}{5.1 \text{ fb}^{-1} + 19.6 \text{ fb}^{-1}} = 1.022 \text{ pb}. \quad (30)$$

For other production modes we get

$$\sigma(\text{ggF})_{\text{weighted}} = 18.365, \sigma(\text{VBF})_{\text{weighted}} = 1.494, \sigma(\text{ttH})_{\text{weighted}} = 0.118 \text{ pb}. \quad (31)$$

By using the weighted cross sections, we obtain the decomposition coefficients $C_{\mathcal{QP}}$ (19) for:

- (i) “untagged” channel of CMS in Table I,
- (ii) “Inclusive” channels in Table II and Table III,
- (iii) “ $\mu(\text{VBF} + \text{VH}, \tau\tau)$ ” channel in Table V under the assumption that the ggF and ttH production modes do not contribute.

For the decomposition coefficients for “0/1 jet” and “VBF tag” in Table V, we take the results for the three search channels $\mu\tau_h + X$, $e\tau_h + X$, and $e\mu + X$, presented in Tables 1, 2, and 3 of Ref.[15].

where n is the degrees of freedom and

$$f(z; n) = \frac{z^{n/2-1} e^{-z/2}}{2^{n/2} \Gamma(n/2)}.$$

For the CMS “VBF tagged” channel in Table I and the “0/1 jet” and “VBF tag” channels in Table III, we borrow the numbers found in Ref. [47].

The Tevatron decomposition coefficients in Tables I and III are from the ratios of the SM Higgs production cross sections. Note that we do not use the Tevatron $\tau\tau$ data upon the large uncertainty recently reported in Ref. [81].

IV. CP CONSERVING FITS

In the CP conserving fits, we have fixed

$$C_{u,d,\ell}^P = \Delta P^{g,\gamma} = 0, \quad (32)$$

while varying

$$C_{u,d,\ell}^S, \quad C_v, \quad \Delta S^{g,\gamma}, \quad \Delta\Gamma_{\text{tot}}. \quad (33)$$

More precisely we have implemented the following 5 fits:

- A. SM fit.
- B. One-parameter fit varying $\Delta\Gamma_{\text{tot}}$ with $C_{u,d,\ell}^S = C_v = 1$ and $\Delta S^{g,\gamma} = 0$.
- C. Two/three-parameter fit varying ΔS^g and ΔS^γ without/with $\Delta\Gamma_{\text{tot}}$ taking $C_{u,d,\ell}^S = C_v = 1$.
- D. Four-parameter fit varying $C_{u,d,\ell}^S$ and C_v with $\Delta S^{g,\gamma} = 0$ and $\Delta\Gamma_{\text{tot}} = 0$.
- E. Six-parameter fit varying $C_{u,d,\ell}^S$, C_v , and $\Delta S^{g,\gamma}$ with $\Delta\Gamma_{\text{tot}} = 0$.

As mentioned above we are going to show the fitting results with the data set *before* and *after* the Moriond 2013 meetings for each fit. Due to the change in the data, especially the diphoton data from the CMS, the fitting results change dramatically. In each of the fits, we first describe the fitting results with respect to the data after the *Hadron Collider Physics Symposium 2012* but before the Moriond 2013; then the fitting results with respect to the data after the Moriond 2013. The best-fit values for the parameters of the above fits are all summarized in Table VI.

The figures are shown for the fits with the most updated data after Moriond. Note also that when we show the 2D χ^2 regions for two of the varying parameters in the figures, we

are marginalizing over the other parameters if more than two are allowed to vary. This also applies to the next section of CP violating fits.

A. SM fit

1. Before Moriond

As we have mentioned the SM fit gives a $\chi^2/dof = 17.5/22 = 0.8$, It gives a p -value of $p = 0.74$, which means the SM has a chance of 0.74 to be the true interpretation of the data. Contributions of chi-square from each data are shown in the second last column of Tables I-V. The $H \rightarrow \gamma\gamma$ data from ATLAS, CMS, and Tevatron give the largest contribution to the chi-square, while the least contribution is from $H \rightarrow ZZ^*$. Specifically, in each decay channel the largest contribution is from: ATLAS $\mu_{ggH+ttH}$ and Tevatron ($H \rightarrow \gamma\gamma$); CMS Inclusive ($H \rightarrow ZZ^*$); CMS VBF tag ($H \rightarrow WW^*$); ATLAS VH tag ($H \rightarrow b\bar{b}$); ATLAS $\mu(ggF, VBF+VH)$ ($H \rightarrow \tau\tau$). As we shall see soon that because the chi-square is dominated by the diphoton data the most efficient way to fit to the data is using ΔS^γ and ΔS^g .

2. After Moriond

The SM fit gives a $\chi^2/dof = 18.94/22 = 0.86$, which gives a p -value of $p = 0.65$. This value shows that the SM description of the data stays more or less the same as before the Moriond update. The diphoton data still dominate the total χ^2 . The χ^2 of each decay channel, shown in the last column of Tables I-V, is about the same as before.

B. Vary only $\Delta\Gamma_{\text{tot}}$ while keeping $C_u^S = C_d^S = C_\ell^S = C_v = 1$ and $\Delta S^\gamma = \Delta S^g = 0$

1. Before Moriond

We found that varying $\Delta\Gamma$ alone does not improve the chi-square. Numerically the chi-square per dof is 17.5/21 and the 95% allowed range for $\Delta\Gamma_{\text{tot}}$ is

$$-0.022_{-0.85}^{+1.44} \text{ MeV} .$$

The central value is consistent with zero and thus the 95% CL upper limit for $\Delta\Gamma_{\text{tot}}$ is about 1.4 MeV. Note that the total width of the SM Higgs boson with $M_H = 125.5$ GeV is about

4.1 – 4.2 MeV. Therefore, the 95% CL upper limit for the nonstandard branching ratio of the Higgs boson is about 25%. The nonstandard decays include invisible decays, decays into other lighter Higgs bosons, or decays into other exotic particles.

2. After Moriond

The situation remains the same. The $\chi^2/dof = 18.89/21$ and the 95% allowed range for $\Delta\Gamma_{\text{tot}}$ is

$$0.10_{-0.74}^{+1.11} \text{ MeV} .$$

The central value is consistent with zero and thus the 95% CL upper limit for $\Delta\Gamma_{\text{tot}}$ is about 1.2 MeV. Therefore, the 95% CL upper limit for the nonstandard branching ratio of the Higgs boson is about 22%.

C. Vary ΔS^γ and ΔS^g while keeping $C_u^S = C_d^S = C_\ell^S = C_v = 1$

1. Before Moriond

In this fit, only the parameters ΔS^γ and ΔS^g vary, which is simply motivated by the fact that the most deviated Higgs data are the diphoton signal strengths while all the other data are more or less consistent with the SM values. It turns out that this is the most efficient way to fit to the data statistically (the most efficient here means that the χ^2 is reduced the most with the best χ^2/dof .) The best fit values are

$$\Delta S^\gamma = -2.73_{-1.15}^{+1.11}, \quad \Delta S^g = -0.050_{-0.065}^{+0.064}, \quad \chi^2/dof = 11.27/20 = 0.56 \quad (34)$$

There are two solutions of ΔS^g , which can be easily understood from the expression of S^g in Eq. (8). Since the signal strengths depend on the absolute value of S^g , numerically, $\pm 0.6 \simeq 0.65 + \Delta S^g$, which gives $\Delta S^g \simeq -0.05$ or -1.25 . They both give $C_g \simeq 0.92$. Also, were to extend the range of ΔS^γ further, there would have been a solution around $\Delta S^\gamma \simeq 16$, according to the expression of S^γ in Eq. (5). Nevertheless, it is unrealistic to find a model that can generate such a large ΔS^γ . The quantities C_γ and C_g are very close to physical observables, and so their best values are

$$C_\gamma \simeq 1.41, \quad C_g \simeq 0.92 .$$

The chi-square per dof for this two-parameter fit is 0.56 compared to 0.8 of the SM, which shows some real improvement.

If we further allow $\Delta\Gamma_{\text{tot}}$ to vary simultaneously with ΔS^γ and ΔS^g , the best fit is

$$\Delta S^\gamma = -2.93_{-1.31}^{+1.19}, \quad \Delta S^g = 0.0063_{-0.11}^{+0.15}, \quad \Delta\Gamma_{\text{tot}} = 0.79_{-1.1}^{+2.0} \text{ MeV}, \quad \chi^2/dof = 10.83/19 = 0.57.$$

It is clear that including $\Delta\Gamma_{\text{tot}}$ in the fit does not improve the chi-square per dof. Since $\Delta\Gamma_{\text{tot}}$ is still consistent with zero in this case, we will fix $\Delta\Gamma_{\text{tot}} = 0$ in the later fits.

2. After Moriond

The most obvious difference between the data set before and after the Moriond 2013 can be seen here in this fit. Before the Moriond the χ^2 is dominated by the diphoton data, in which both ATLAS and CMS showed $1.5 - 2\sigma$ excesses, and so the dynamics of the fit will push to the direction to substantially reduce the χ^2 of the diphoton data. However, with the new CMS diphoton data ($0.78_{-0.26}^{+0.28}$) the whole fit changes. The dynamics of the fit cannot force the parameters to go into one direction, because the ATLAS data is still about 1.5σ larger than the SM while the CMS one is about 1σ smaller.

The best fit values for ΔS^γ and ΔS^g are

$$\Delta S^\gamma = -0.96_{-0.85}^{+0.84}, \quad \Delta S^g = -0.043 \pm 0.052, \quad \chi^2/dof = 17.55/20 = 0.88 \quad (35)$$

We notice that the sizes of the errors are reduced reflecting more precise measurements of the Higgs data. The distributions of chi-square in the plane of $(\Delta S^\gamma, \Delta S^g)$ and the corresponding (C_γ, C_g) plane are shown in Fig. 1(a) and (b), respectively. The quantities C_γ and C_g are very close to physical observables, and so their best values are

$$C_\gamma \simeq 1.14, \quad C_g \simeq 0.93 .$$

The chi-square per dof for this two-parameter fit is 0.88 compared to 0.86 of the SM. The p -values are very similar.

Again, we further allow $\Delta\Gamma_{\text{tot}}$ to vary simultaneously with ΔS^γ and ΔS^g , the best fit is

$$\Delta S^\gamma = -0.96_{-0.87}^{+0.84}, \quad \Delta S^g = -0.040_{-0.086}^{+0.12}, \quad \Delta\Gamma_{\text{tot}} = 0.027_{-0.80}^{+1.33} \text{ MeV}, \quad \chi^2/dof = 17.55/19 = 0.92.$$

The 2-dim contours for the correlations among the 3 parameters are shown in Fig. 2. Note that anticorrelation between C_γ and C_g shown in Fig. 1(b) is modified to the shape shown

in Fig. 2(d). The elongation along the C_g is allowed with the increase in $\Delta\Gamma_{\text{tot}}$ such that the production in ggF increases but the decays in various channels decrease. It is clear that including $\Delta\Gamma_{\text{tot}}$ in the fit does not improve the fit.

It is easy to notice that ΔS^γ and ΔS^g were very efficient in reducing the χ^2 of the Higgs data *before* the Moriond update, because both the ATLAS and CMS had the diphoton data on the excess side of the SM value. However, *after* the Moriond update the CMS diphoton data is smaller than the SM value while the ATLAS is still larger, and therefore the χ^2 cannot be reduced effectively no matter how ΔS^γ and ΔS^g are varied.

D. Vary $C_u^S, C_d^S, C_\ell^S, C_v$ while keeping $\Delta S^\gamma = \Delta S^g = 0$

This choice is motivated in the scenario where there are no new particles running in the triangular loops of Higgs boson decaying into gg or $\gamma\gamma$, but only modifications of Yukawa couplings. It can be realized in a two-Higgs doublet model with a very heavy charged Higgs boson and modifications of Yukawa couplings can be expressed in terms of the mixing angle α and $\tan\beta$.

First, we notice that there is an overall symmetry:

$$C_u^S \leftrightarrow -C_u^S, C_d^S \leftrightarrow -C_d^S, C_\ell^S \leftrightarrow -C_\ell^S, C_v \leftrightarrow -C_v$$

simply obtained by flipping the overall sign in Eqs. (1) and (2). Furthermore, from Eq. (5) the diphoton production rate depends on $|S^\gamma|^2 + |P^\gamma|^2$, and so only the relative signs of gauge and Yukawa couplings are important. Therefore, in the following we fix the sign of C_v to be positive, while the other 3 parameters can be either negative or positive.

Since the contributions of the bottom and the charged-lepton sectors to the diphotons are very small, we expect an approximate symmetry: $C_d^S \leftrightarrow -C_d^S$ and $C_\ell^S \leftrightarrow -C_\ell^S$. Even if we change the best-fit point by $C_\ell^S \rightarrow -C_\ell^S$ the total χ^2 only changes by $O(+0.01)$. This simply means that changing the sign of bottom- and charged-lepton Yukawa couplings would not affect significantly the loop contributions of $H\gamma\gamma$ and Hgg . We show in Fig. 3 the 2-dim contours for the correlations of any 2 of the 4 parameters ($C_u^S, C_d^S, C_\ell^S, C_v$). In the figure, we can see an approximate symmetry: $C_d^S \leftrightarrow -C_d^S$ and $C_\ell^S \leftrightarrow -C_\ell^S$. Note that this figure is for the data after the Moriond update.

On the other hand, the sign of C_u^S is important, as shown by the two islands in the panel

(a). It is well known that the SM W boson and top quark loop contributions to $H\gamma\gamma$ come in opposite sign. Therefore, by flipping the sign of the top quark contribution ($C_u^S \rightarrow -C_u^S$) it can enhance the $H\gamma\gamma$ vertex.

1. Before Moriond

Since before the Moriond update both the CMS and ATLAS diphoton data are in excess, the dynamics of the fit indeed prefers $C_u^S < 0$ for positive C_v , shown in the fifth column of the upper half of Table VI. In this way, the diphoton rate is pushed up to fit well with the data and significantly reduces the χ^2 . Thus results in $\chi^2/dof = 10.46/18$.

2. After Moriond

Nevertheless, the new CMS diphoton data affect the fit significantly. The dynamics of the fit cannot force the parameters to go into one direction to reduce the χ^2 , because the ATLAS diphoton data is on the opposite side of the CMS data. Thus, the top-Yukawa $C_u^S \approx 0.8$ (see the fifth column of the lower half of Table VI), which means that the top contribution to the $H\gamma\gamma$ vertex is only reduced by a small amount. Therefore, we only obtain an overall $\chi^2/dof = 17.82/18 = 0.99$, which is worse than the SM fit.

In Fig. 4(a), we show the corresponding confidence-level regions in the (C_γ, C_g) plane. The central values are $C_\gamma = 1.09, C_g = 0.91$. Note that original anticorrelation between C_γ and C_g shown in Fig. 1(b) is modified to the shape shown in Fig. 4(a). The enlargement region in C_g can be understood when C_u^S increases, C_g will increase but C_γ is reduced such that the diphoton rate stays about the same. Another enlargement region in C_γ direction can be understood as the left island of Fig. 3(a), in which C_u^S is negative, such that C_γ is large and C_g is about the same. In part (b), we show the correlation between C_γ and $C_{Z\gamma}$. There are 2 islands corresponding to those shown in Fig. 3(a). Both C_γ and $C_{Z\gamma}$ increase or decrease in the same direction, though the enhancement in $C_{Z\gamma}$ is always smaller than C_γ . At the best-fit point, we find $C_{Z\gamma} = 1.05$.

E. Vary $C_u^S, C_d^S, C_\ell^S, C_v, \Delta S^\gamma, \Delta S^g$

In this fit, we group these 6 parameters into 2 sets: $(C_u^S, C_d^S, C_\ell^S, C_v)$ and $(\Delta S^\gamma, \Delta S^g)$. We first show the correlations among the first set in Fig. 5, which can be compared directly to the corresponding panels in Fig. 3. It is easy to see that all the confidence-level regions are enlarged due to more dof in $(\Delta S^\gamma, \Delta S^g)$. The next correlations between (C_u^S, C_v) and $(\Delta S^\gamma, \Delta S^g)$ are shown in Fig. 6. The correlations between (C_d^S, C_ℓ^S) and $(\Delta S^\gamma, \Delta S^g)$ are shown in Fig. 7. The corresponding confidence-level regions in $(\Delta S^\gamma, \Delta S^g)$ and (C_γ, C_g) planes are shown in Fig. 8. Note that these figures used the data after the Moriond update.

1. Before Moriond

The fit before Moriond is shown in the last column of the upper half in Table VI. The most significant changes from the previous fit are the widening of C_u^S and the shift of the best value of C_u^S from approximately $-0.9 \rightarrow 0$. We shall explain it shortly. The C_v and C_d^S remains approximately the same. Although the C_ℓ^S flips the sign, the absolute value is about the same. The flipping of the sign of C_ℓ^S is simply a numerical artifact that the difference in χ^2 is only $O(10^{-3})$. In this 6-parameter fit, the signs of the best values of $C_u^S, C_d^S, C_\ell^S, C_v$ are all positive, in accord with the SM.

The shift of C_u^S from $-0.9 \rightarrow 0$ can be understood from the numerical expression of S^γ in Eq. (5). In the 4-parameter fit where $\Delta S^\gamma = 0$, the top-Yukawa coupling C_u^S is made negative in order to increase numerically the S^γ ; whereas in the 6-parameter fit the C_u^S goes to zero and ΔS^γ goes to a negative value to enhance S^γ . This explains the shift of C_u^S and anti-correlation between C_u^S and ΔS^γ .

The resulting $\chi^2/dof = 9.89/16$, which is pretty good. The dynamics of the fit raises the diphoton rate to fit the data well, so that the χ^2 is reduced substantially.

2. After Moriond

As shown in the last column of the lower half in Table VI, the C_u^S changes from approximately $0.8 \rightarrow 0$, while the C_d^S, C_ℓ^S , and C_v remains about 1. The Yukawa couplings are almost in good accord with the SM, except for the top-Yukawa. Instead, ΔS^γ and ΔS^g

become nonzero to accommodate the data. Nevertheless, the reduction of χ^2 is very small. The resulting $\chi^2/dof = 16.89/16$, which is worse than all other fits.

The next correlations between (C_u^S, C_v) and $(\Delta S^\gamma, \Delta S^g)$ are shown in Fig. 6. Both the ΔS^γ and ΔS^g are anti-correlated with C_u^S . On the other hand, ΔS^γ and ΔS^g do not correlate with C_v . Similarly, the correlations between (C_d^S, C_ℓ^S) and $(\Delta S^\gamma, \Delta S^g)$ are shown in Fig. 7, which are also negligibly correlated.

The corresponding confidence-level regions in $(\Delta S^\gamma, \Delta S^g)$ and (C_γ, C_g) planes are shown in Fig. 8. The prediction for $C_{Z\gamma}$ is also shown. Again, the $C_{Z\gamma}$ increases or decreases in the same direction as C_γ , but is always smaller than C_γ .

F. Concluding remarks

The best-fit values for various CP-conserving fits using the Higgs data before the Moriond 2013 are shown in the upper half of Table VI while using the data after the Moriond are shown in the lower half. We also show the p -value of each fit. It is clear that most of the fits have better p -values than the SM one before the Moriond; while all the fits are worse than the SM one after the Moriond.

Before the Moriond update, the diphoton signal strength $pp \rightarrow H \rightarrow \gamma\gamma$ dominates the chi-square. Both the ATLAS and CMS diphoton data are on the *same* side of excess of the SM value. The signal strength of $pp \rightarrow H \rightarrow \gamma\gamma$ depends largely on S^γ and S^g , which in turns depend mostly on C_u^S and ΔS^γ . Indeed, we have shown in the 4-parameter analysis and in the 6-parameter analysis, the χ^2 is mostly sensitive to C_u^S and ΔS^γ . In the 4-parameter analysis where $\Delta S^\gamma = 0$, the best-fit value of $C_u^S \approx -0.9$ in order to enhance S^γ ; whereas in the 6-parameter analysis $C_u^S \approx 0$ and $\Delta S^\gamma \approx -1.2$ are preferred in order to enhance S^γ . The value for ΔS^g also changes according to the change in the value of C_u^S as in the expression for S^g in Eq. (8).

The C_u^S and ΔS^γ are the two parameters most sensitive to the signal strength of $pp \rightarrow H \rightarrow \gamma\gamma$. Keeping the other parameters as $C_v = C_d^S = C_\ell^S = 1, \Delta S^g = 0, \Delta\Gamma_{\text{tot}} = 0$, we vary C_u^S and ΔS^γ only and we find the best-fit values are

$$C_u^S = 0.92_{-0.095}^{+0.094}, \quad \Delta S^\gamma = -2.62_{-1.04}^{+1.02}, \quad \chi^2/dof = 11.17/20. \quad (36)$$

This is the best χ^2/dof that we found when only two parameters are allowed to vary,

although the total χ^2 is only 0.1 unit better than the fit with ΔS^γ and ΔS^g , which is statistically insignificant.

With the Higgs updates during the Moriond 2013 meetings [24] the uncertainties in most channels are reduced. The decay channels other than the diphoton also began to play important roles in the global fits. The most dramatic change is the CMS diphoton data, in which the central value (the untagged) changes from 1.42 to 0.78. Now the CMS and ATLAS diphoton data are on the *opposite* side of the SM value. The dynamics of the fit cannot do anything to effectively reduce the χ^2 from the diphoton data. We found that all the fits give a p -value worse than the SM one.

V. CP VIOLATING FITS

We devote this section to including the pseudoscalar Yukawa couplings and the pseudoscalar contributions ΔP^γ and ΔP^g .

A. ΔS^γ , ΔS^g , ΔP^γ and ΔP^g

1. Before Moriond

We have learned from all CP-conserving fits in the last section that the most efficient parameters fitting the data are the deviation ΔS^γ to the $H\gamma\gamma$ vertex and the up-type Yukawa coupling C_u^S , as well as the corresponding deviation ΔS^g to the Hgg vertex. In order to understand the effects of pseudoscalar nature of the Higgs boson, we first perform the analysis by varying the scalar contributions ΔS^γ and ΔS^g , as well as the pseudoscalar contributions ΔP^γ and ΔP^g to the $H\gamma\gamma$ and Hgg vertices. We keep all other parameters at the SM values, $C_u^S = C_d^S = C_\ell^S = C_v = 1$, $C_u^P = C_d^P = C_\ell^P = 0$ and $\Delta\Gamma_{\text{tot}} = 0$.

The best-fit parameters and the corresponding χ^2 for this case are shown in the second and third columns of the upper half in Table VII. The total $\chi^2 = 11.26$, almost the same as the total $\chi^2 = 11.27$ of the case varying $\Delta S^\gamma, \Delta S^g$ only. Therefore, including the pseudoscalar contributions does not improve the fit at all. In fact, the χ^2/dof is worsened.

2. After Moriond

The confidence-level regions in the $(\Delta S^g, \Delta P^g)$, in the $(\Delta S^\gamma, \Delta P^\gamma)$, and in the corresponding (C_γ, C_g) planes are shown in Fig. 9. The nearly-physical values for $C_\gamma \approx 1.1$ and $C_g \approx 0.9$, which are the same as the fit using just ΔS^γ and ΔS^g . In order to understand the behavior shown in Fig. 9(a) and (b), we can use the numerical expressions for S^γ, P^γ in Eq. (5) and S^g, P^g in Eq. (8).

Numerically,

$$C_\gamma \approx 1.1 = \sqrt{\frac{(-6.64 + \Delta S^\gamma)^2 + (\Delta P^\gamma)^2}{(-6.64)^2}},$$

$$C_g \approx 0.9 = \sqrt{\frac{(0.65 + \Delta S^g)^2 + (\Delta P^g)^2}{(0.65)^2}}.$$

Therefore, we obtain 2 ellipses

$$(7.3)^2 = (-6.64 + \Delta S^\gamma)^2 + (\Delta P^\gamma)^2,$$

$$(0.59)^2 = (0.65 + \Delta S^g)^2 + (\Delta P^g)^2. \quad (37)$$

that explain the ellipses shown in Fig. 9(a) and (b). It is clear that nonzero values of ΔP^γ and ΔP^g are not ruled out, and the data allow for both scalar and pseudoscalar values in special combinations for $H\gamma\gamma$ and Hgg vertices.

The best-fit parameters and the corresponding χ^2 for this case are shown in the second and third columns of the lower half in Table VII. The total $\chi^2 = 17.55$, the same as the case varying $\Delta S^\gamma, \Delta S^g$ only. Again, including the pseudoscalar contributions does not improve the fit at all.

B. C_u^S, C_u^P and C_v

From the results of the last section, we can see that among all the Yukawa couplings the fitting result is more sensitive to the up-type Yukawa couplings C_u^S . This is easy to understand because the diphoton data currently dominate the chi-square, and the top-Yukawa and HWW couplings are the most important to determine the diphoton signal strength. Without loss of generality we only consider the up-type scalar and pseudoscalar Yukawa couplings and C_v in this subsection. The effects of down-type and charged-lepton pseudoscalar couplings are similar but much milder.

1. Before Moriond

The best-fit parameters and the corresponding χ^2 for this case are shown in the fourth and the fifth columns of the upper half in Table VII. The total $\chi^2 = 10.53$, almost the same as the total $\chi^2 = 10.46$ of the case varying $C_{u,d,\ell}^S$ and C_v . Therefore, including the pseudoscalar Yukawa coupling C_u^P does not improve the fit. Nevertheless, the p -values are about the same, and so the data cannot rule out the combination of scalar and pseudoscalar Yukawa couplings.

2. After Moriond

The 2-dim confidence-level regions among the parameters (C_u^S, C_u^P, C_v) are shown in Fig. 10. We can directly compare Fig. 3(a) and Fig. 10(a). The 2 islands in Fig. 3(a) are now linked together in Fig. 10(a), due to the variation of an additional parameter C_u^P . The sickle-shaped region in part (c) indicates that C_u^S and C_u^P satisfy some equations of ellipses. From the numerical expressions for S^γ, P^γ in Eq. (5) and S^g, P^g in Eq. (8), we have

$$\begin{aligned} (7.3)^2 &= (-8.4 + 1.76 C_u^S)^2 + (2.78 C_u^P)^2 \\ (0.59)^2 &= (0.688 C_u^S)^2 + (1.047 C_u^P)^2 \end{aligned} \quad (38)$$

which can then explain the shape in part (c).

The correlation between C_γ and $C_{Z\gamma}$ is shown in part (e) and that for the CP-violating observables, which are proportional to $2C_u^S C_u^P / (C_u^{S^2} + C_u^{P^2})$, is shown in part (f). The $C_{Z\gamma}$ increases and decreases in the same direction as C_γ but always smaller than C_γ . At the best-fit point, $C_\gamma \approx 1.1$ while $C_{Z\gamma} \approx 1.05$. The CP-violating observables arised from the mixing between scalar and pseudoscalar contributions are in general proportional to $2C_u^S C_u^P / (C_u^{S^2} + C_u^{P^2})$.

The best-fit parameters and the corresponding χ^2 for this case are shown in the fourth and the fifth columns of the lower half in Table VII. The p -value is slightly better than the CP-conserving case of varying $C_{u,d,\ell}^S$ and C_v .

VI. DISCUSSION

In this work, we have established a model-independent framework that enables one to analyze all the observed Higgs boson signal strengths and to fit to the Higgs boson couplings to fermions, W/Z bosons, $\gamma\gamma$, and gg . In the future when the $Z\gamma$ data are available, the current framework can also cover that. Right now we give predictions for $Z\gamma$ signal strengths. We have performed global fits to all the Higgs signal strengths recorded by ATLAS, CMS, and at the Tevatron. Furthermore, we have also performed fits including the pseudoscalar up-type Yukawa coupling C_u^P and the pseudoscalar contributions P^γ and P^g in the $H\gamma\gamma$ and Hgg vertices, respectively.

Furthermore, we have performed fits with respect to all the Higgs data collected *before* and *after* the Moriond 2013 meetings. The main reason why we separately performed them is because of the dramatic change in the fits due to the shift of the CMS diphoton data from 1.42 to 0.78 of the SM value. Before the Moriond update the dynamics of the fit pushes the parameters to increase the diphoton rate such that the χ^2 is reduced effectively. However, with all the data after the Moriond the dynamics of the fit cannot find the optimal set of parameters so that the resulting χ^2/dof 's are indeed worse than the SM.

In summary, the p -value of the SM Higgs boson is 0.65 performed with all the data after the Moriond. Its p -value is higher than any other fits considered in this work, both the CP conserving ones and the CP-violating ones. We also plot the p -values for all the fits considered in this work in Fig. 11.

Our findings are summarized as follows.

1. Before the Moriond, the SM already enjoyed a good $\chi^2/dof = 0.8$ (p -value = 0.74), which means that the SM Higgs description of the data is reasonably well. Out of the total $\chi^2 = 17.5$ about one half comes from the $H \rightarrow \gamma\gamma$ data. Similarly, after the Moriond the SM has $\chi^2/dof = 0.86$ (p -value = 0.65).
2. If only the total Higgs boson width is allowed to vary, we are able to constrain the deviation $\Delta\Gamma_{\text{tot}}$ to be less than 1.2 MeV at 95%CL. Given the SM Higgs boson width is about 4.1 – 4.2 MeV for $M_H = 125 - 126$ GeV, the nonstandard decay branching ratio of the Higgs boson is less than 22% at 95% CL. This is a real improvement from previous estimates of about 40% [82].

3. The most efficient set of parameters to fit to the data before the Moriond are the additional particle contributions to the loop functions of $H\gamma\gamma$ and Hgg vertices, ΔS^γ and ΔS^g respectively. This is because both the ATLAS and CMS have diphoton data above the SM value. The best χ^2/dof obtained is about 0.56. This is easy to understand, as the total χ^2 is currently dominated by $H \rightarrow \gamma\gamma$ signal strength. Nevertheless, with the Moriond update the CMS diphoton data is now below the SM value. No optimal set of parameters can be found to effectively reduce the total χ^2 .
4. With the data before the Moriond, another efficient set of parameters are C_u^S and ΔS^γ . We found that they are equally effective as $(\Delta S^\gamma, \Delta S^g)$. Effectively, the modification in C_u^S takes up the place of ΔS^g . Again, the reason is the domination of $H \rightarrow \gamma\gamma$ in the total χ^2 . Nevertheless, after the Moriond update no optimal set of parameters can be found.
5. The relative HVV coupling now stands at $C_v = 1.01^{+0.13}_{-0.14}$ in the 6-parameter fit (and a similar value in the 4-parameter fit). This implies that the observed Higgs boson accounts for most of the EWSB, and leaves little rooms for additional Higgs bosons that are also responsible for EWSB. Nevertheless, if we take -2σ to the central value, the C_v can be as low as 0.7. The vector-boson scattering could become strong if the UV part of the Higgs sector is very heavy [83].
6. The current data do not rule out the pseudoscalar contributions to the $H\gamma\gamma$ and Hgg vertices nor the pseudoscalar Yukawa couplings. Nevertheless, including pseudoscalar contributions to $H\gamma\gamma$ and Hgg vertices or pseudoscalar Yukawa couplings do not improve the fits. The current Higgs observables are not sensitive to CP-violating effects, and so only combinations of scalar and pseudoscalar contributions are constrained, as shown in Eqs. (37) and (38). Thus, the current Higgs data do not rule out or favor pseudoscalar couplings.

Era of Higgs-boson precision studies now begins – Higgcision. In this work, we have already seen dramatic changes in the fits with the data collected *before* and *after* the Moriond 2013. We are looking forward to more and more data in the upcoming Summer 2013 and the following years.

ACKNOWLEDGMENT

This work was supported the National Science Council of Taiwan under Grants No. 99-2112-M-007-005-MY3 and the WCU program through the KOSEF funded by the MEST (R31-2008-000-10057-0). This study was financially supported by Chonnam National University, 2012/2013. J.S.L thanks National Center for Theoretical Sciences (Hsinchu, Taiwan) for the great hospitality extended to him while this work was being performed.

-
- [1] G. Aad *et al.* [ATLAS Collaboration], Phys. Lett. B **716**, 1 (2012) [arXiv:1207.7214 [hep-ex]].
 - [2] S. Chatrchyan *et al.* [CMS Collaboration], Phys. Lett. B **716**, 30 (2012) [arXiv:1207.7235 [hep-ex]].
 - [3] P. W. Higgs, Phys. Rev. Lett. **13**, 508 (1964); F. Englert and R. Brout, Phys. Rev. Lett. **13**, 321 (1964); G. S. Guralnik, C. R. Hagen and T. W. B. Kibble, Phys. Rev. Lett. **13**, 585 (1964).
 - [4] G. Aad *et al.* [ATLAS Collaboration], Phys. Lett. B **710**, 49 (2012) [arXiv:1202.1408 [hep-ex]]; S. Chatrchyan *et al.* [CMS Collaboration], Phys. Lett. B **710**, 26 (2012) [arXiv:1202.1488 [hep-ex]].
 - [5] T. Aaltonen *et al.* [CDF and D0 Collaborations], Phys. Rev. Lett. **109**, 071804 (2012) [arXiv:1207.6436 [hep-ex]].
 - [6] Talk presented by K. Einsweiler (ATLAS) at HCP2012, 15 Nov 2012, Kyoto, Japan; Talk presented by C. Paus (CMS) at HCP2012, 15 Nov 2012, Kyoto, Japan.
 - [7] Aurelio Juste, “Standard Model Higgs boson searches at the Tevatron”, talk at HCP2012, 15 Nov 2012, Kyoto, Japan,
<http://kds.kek.jp/conferenceDisplay.py?confId=9237>.
 - [8] Yuji Enari, “ $H \rightarrow b\bar{b}$ from Tevatron”, talk at HCP2012, 14 Nov 2012, Kyoto, Japan,
<http://kds.kek.jp/conferenceDisplay.py?confId=10808>.
 - [9] ATLAS-CONF-2012-168, “Observation and study of the Higgs boson candidate in the two photon decay channel with the ATLAS detector at the LHC” (Dec 2012).
 - [10] ATLAS-CONF-2012-170, “An update of combined measurements of the new Higgs-like boson with high mass resolution channels” (Dec 2012).

- [11] ATLAS-CONF-2012-160, “Search for the Standard Model Higgs boson in $H \rightarrow \tau^+\tau^-$ decays in proton-proton collisions with the ATLAS detector” (Nov 2012).
- [12] ATLAS-CONF-2012-169, “Updated results and measurements of properties of the new Higgs-like particle in the four lepton decay channel with the ATLAS detector” (Dec 2012).
- [13] CMS-PAS-HIG-12-045, “Combination of standard model Higgs boson searches and measurements of the properties of the new boson with a mass near 125 GeV” (Nov 2012).
- [14] CMS-PAS-HIG-12-041, “Updated results on the new boson discovered in the search for the standard model Higgs boson in the $H \rightarrow ZZ \rightarrow 4l$ channel in pp collisions at $\sqrt{s} = 7$ and 8 TeV” (Nov 2012).
- [15] CMS-PAS-HIG-12-043, “Search for the standard model Higgs boson decaying to tau pairs”(Nov 2012).
- [16] See for example, M. Carena, S. Gori, N. R. Shah and C. E. M. Wagner, JHEP **1203**, 014 (2012) [arXiv:1112.3336 [hep-ph]];
- [17] See for example, U. Ellwanger, JHEP **1203**, 044 (2012) [arXiv:1112.3548 [hep-ph]];
- [18] C. -F. Chang, K. Cheung, Y. -C. Lin and T. -C. Yuan, JHEP **1206** 128 (2012), [arXiv:1202.0054 [hep-ph]]; K. Cheung, C. -T. Lu and T. -C. Yuan, arXiv:1212.1288 [hep-ph].
- [19] E. Gabrielli, B. Mele and M. Raidal, arXiv:1202.1796 [hep-ph];
- [20] P. M. Ferreira, R. Santos, M. Sher and J. P. Silva, Phys. Rev. D **85**, 077703 (2012) [arXiv:1112.3277 [hep-ph]];
- [21] See for example, K. Cheung and T. -C. Yuan, Phys. Rev. Lett. **108**, 141602 (2012) [arXiv:1112.4146 [hep-ph]];
- [22] A. Arhrib, R. Benbrik and N. Gaur, Phys. Rev. D **85**, 095021 (2012) [arXiv:1201.2644 [hep-ph]].
- [23] J. Chang, K. Cheung, P. -Y. Tseng and T. -C. Yuan, arXiv:1206.5853 [hep-ph]; Int. J. Mod. Phys. A **27**, 1230030 (2012) [arXiv:1211.6823 [hep-ph]].
- [24] The XLVIIIth Rencontres de Moriond: the Electroweak Interactions and Unified Theories; and QCD and High Energy Interactions (<http://moriond.in2p3.fr/>).
- [25] The ATLAS Collaboration, ATLAS-CONF-2013-012, “Measurements of the properties of the Higgs-like boson in the two photon decay channel with the ATLAS detector using 25 fb⁻¹ of proton-proton collision data” (Mar. 2013).

- [26] The ATLAS Collaboration, ATLAS-CONF-2013-034, “Combined coupling measurements of the Higgs-like boson with the ATLAS detector using up to 25 fb^{-1} of proton-proton collision data” (Mar. 2013).
- [27] The CMS Collaboration, CMS PAS HIG-13-001, “Updated measurements of the Higgs boson at 125 GeV in the two photon decay channel” (Mar. 2013).
- [28] The CMS Collaboration, CMS PAS HIG-13-002, “Properties of the Higgs-like boson in the decay $H \rightarrow ZZ \rightarrow 4l$ in pp collisions at $\sqrt{s} = 7$ and 8 TeV” (Mar. 2013).
- [29] The CMS Collaboration, CMS PAS HIG-13-003, “Update on the search for the standard model Higgs boson in pp collisions at the LHC decaying to W^+W^- in the fully leptonic final state” (Mar. 2013).
- [30] The CMS Collaboration, CMS PAS HIG-13-004, “Search for the Standard-Model Higgs boson decaying to tau pairs in proton-proton collisions at $\sqrt{s} = 7$ and 8 TeV” (Mar. 2013).
- [31] D. Carmi, A. Falkowski, E. Kuflik and T. Volansky, JHEP **1207**, 136 (2012) [arXiv:1202.3144 [hep-ph]].
- [32] A. Azatov, R. Contino and J. Galloway, JHEP **1204**, 127 (2012) [arXiv:1202.3415 [hep-ph]].
- [33] J. R. Espinosa, C. Grojean, M. Muhlleitner and M. Trott, JHEP **1205**, 097 (2012) [arXiv:1202.3697 [hep-ph]].
- [34] M. Klute, R. Lafaye, T. Plehn, M. Rauch and D. Zerwas, Phys. Rev. Lett. **109**, 101801 (2012) [arXiv:1205.2699 [hep-ph]].
- [35] D. Carmi, A. Falkowski, E. Kuflik and T. Volansky, arXiv:1206.4201 [hep-ph].
- [36] I. Low, J. Lykken and G. Shaughnessy, Phys. Rev. D **86**, 093012 (2012) [arXiv:1207.1093 [hep-ph]].
- [37] P. P. Giardino, K. Kannike, M. Raidal and A. Strumia, Phys. Lett. B **718**, 469 (2012) [arXiv:1207.1347 [hep-ph]].
- [38] J. Ellis and T. You, JHEP **1209**, 123 (2012) [arXiv:1207.1693 [hep-ph]].
- [39] J. R. Espinosa, C. Grojean, M. Muhlleitner and M. Trott, JHEP **1212**, 045 (2012) [arXiv:1207.1717 [hep-ph]].
- [40] D. Carmi, A. Falkowski, E. Kuflik, T. Volansky and J. Zupan, JHEP **1210**, 196 (2012) [arXiv:1207.1718 [hep-ph]].
- [41] S. Banerjee, S. Mukhopadhyay and B. Mukhopadhyaya, JHEP **1210**, 062 (2012) [arXiv:1207.3588 [hep-ph]].

- [42] F. Bonnet, T. Ota, M. Rauch and W. Winter, Phys. Rev. D **86**, 093014 (2012) [arXiv:1207.4599 [hep-ph]].
- [43] T. Plehn and M. Rauch, Europhys. Lett. **100**, 11002 (2012) [arXiv:1207.6108 [hep-ph]].
- [44] A. Djouadi, arXiv:1208.3436 [hep-ph].
- [45] B. A. Dobrescu and J. D. Lykken, arXiv:1210.3342 [hep-ph].
- [46] G. Cacciapaglia, A. Deandrea, G. D. La Rochelle and J. -B. Flament, arXiv:1210.8120 [hep-ph].
- [47] G. Belanger, B. Dumont, U. Ellwanger, J. F. Gunion and S. Kraml, arXiv:1212.5244 [hep-ph].
- [48] G. Moreau, Phys. Rev. D **87**, 015027 (2013) [arXiv:1210.3977 [hep-ph]].
- [49] T. Corbett, O. J. P. Eboli, J. Gonzalez-Fraile and M. C. Gonzalez-Garcia, Phys. Rev. D **86**, 075013 (2012) [arXiv:1207.1344 [hep-ph]].
- [50] T. Corbett, O. J. P. Eboli, J. Gonzalez-Fraile and M. C. Gonzalez-Garcia, Phys. Rev. D **87**, 015022 (2013) [arXiv:1211.4580 [hep-ph]].
- [51] E. Masso and V. Sanz, arXiv:1211.1320 [hep-ph].
- [52] H. S. Cheon and S. K. Kang, arXiv:1207.1083 [hep-ph].
- [53] N. Craig and S. Thomas, JHEP **1211**, 083 (2012) [arXiv:1207.4835 [hep-ph]].
- [54] D. S. M. Alves, P. J. Fox and N. J. Weiner, arXiv:1207.5499 [hep-ph].
- [55] W. Altmannshofer, S. Gori and G. D. Kribs, Phys. Rev. D **86**, 115009 (2012) [arXiv:1210.2465 [hep-ph]].
- [56] S. Chang, S. K. Kang, J. -P. Lee, K. Y. Lee, S. C. Park and J. Song, arXiv:1210.3439 [hep-ph].
- [57] Y. Bai, V. Barger, L. L. Everett and G. Shaughnessy, arXiv:1210.4922 [hep-ph].
- [58] A. Drozd, B. Grzadkowski, J. F. Gunion and Y. Jiang, arXiv:1211.3580 [hep-ph].
- [59] A. Celis, V. Ilisie and A. Pich, arXiv:1302.4022 [hep-ph].
- [60] J. R. Espinosa, C. Grojean, V. Sanz and M. Trott, JHEP **1212**, 077 (2012) [arXiv:1207.7355 [hep-ph]].
- [61] A. Azatov, S. Chang, N. Craig and J. Galloway, Phys. Rev. D **86**, 075033 (2012) [arXiv:1206.1058 [hep-ph]].
- [62] P. Bechtle, S. Heinemeyer, O. Stal, T. Stefaniak, G. Weiglein and L. Zeune, arXiv:1211.1955 [hep-ph].
- [63] J. Cao, Z. Heng, J. M. Yang and J. Zhu, JHEP **1210**, 079 (2012) [arXiv:1207.3698 [hep-ph]].

- [64] H. Baer, V. Barger, P. Huang, D. Mickelson, A. Mustafayev and X. Tata, arXiv:1210.3019 [hep-ph].
- [65] T. Modak, D. Sahoo, R. Sinha and H. -Y. Cheng, arXiv:1301.5404 [hep-ph].
- [66] J. S. Lee, A. Pilaftsis, M. S. Carena, S. Y. Choi, M. Drees, J. R. Ellis and C. E. M. Wagner, “CPsuperH: A Computational tool for Higgs phenomenology in the minimal supersymmetric standard model with explicit CP violation,” *Comput. Phys. Commun.* **156** (2004) 283 [hep-ph/0307377].
- [67] J. S. Lee, M. Carena, J. Ellis, A. Pilaftsis and C. E. M. Wagner, “CPsuperH2.0: an Improved Computational Tool for Higgs Phenomenology in the MSSM with Explicit CP Violation,” *Comput. Phys. Commun.* **180** (2009) 312 [arXiv:0712.2360 [hep-ph]].
- [68] J. S. Lee, M. Carena, J. Ellis, A. Pilaftsis and C. E. M. Wagner, “CPsuperH2.3: an Updated Tool for Phenomenology in the MSSM with Explicit CP Violation,” arXiv:1208.2212 [hep-ph].
- [69] A. Djouadi, V. Driesen, W. Hollik and A. Kraft, “The Higgs photon - Z boson coupling revisited,” *Eur. Phys. J. C* **1** (1998) 163 [hep-ph/9701342].
- [70] M. Gonderinger, Y. Li, H. Patel and M. J. Ramsey-Musolf, *JHEP* **1001**, 053 (2010) [arXiv:0910.3167 [hep-ph]].
- [71] Y. Cai, X. -G. He and B. Ren, *Phys. Rev. D* **83**, 083524 (2011) [arXiv:1102.1522 [hep-ph]].
- [72] A. Drozd, B. Grzadkowski and J. Wudka, *JHEP* **1204**, 006 (2012) [arXiv:1112.2582 [hep-ph]].
- [73] K. Cheung, Y. -L. S. Tsai, P. -Y. Tseng, T. -C. Yuan and A. Zee, *JCAP* **1210**, 042 (2012) [arXiv:1207.4930 [hep-ph]].
- [74] K. Cheung, T. -J. Hou, J. S. Lee and E. Senaha, “The Higgs Boson Sector of the Next-to-MSSM with CP Violation,” *Phys. Rev. D* **82** (2010) 075007 [arXiv:1006.1458 [hep-ph]].
- [75] N. Arkani-Hamed, A. G. Cohen, E. Katz and A. E. Nelson, *JHEP* **0207**, 034 (2002) [hep-ph/0206021].
- [76] T. Han, H. E. Logan, B. McElrath and L. -T. Wang, *Phys. Rev. D* **67**, 095004 (2003) [hep-ph/0301040].
- [77] J. Reuter and M. Tonini, arXiv:1212.5930 [hep-ph].
- [78] X. -F. Han, L. Wang, J. M. Yang and J. Zhu, arXiv:1301.0090 [hep-ph].
- [79] J. Beringer et al. (Particle Data Group), *Phys. Rev.* **D86**, 010001 (2012).
- [80] <https://twiki.cern.ch/twiki/bin/view/LHCPhysics/CrossSections>
- [81] T. Aaltonen *et al.* [CDF Collaboration], arXiv:1301.6668 [hep-ex].

- [82] A. Djouadi, A. Falkowski, Y. Mambrini and J. Quevillon, arXiv:1205.3169 [hep-ph].
- [83] K. Cheung, C. -W. Chiang and T. -C. Yuan, Phys. Rev. D **78**, 051701 (2008) [arXiv:0803.2661 [hep-ph]]; J. Chang, K. Cheung, C. -T. Lu and T. -C. Yuan, arXiv:1303.6335 [hep-ph].

TABLE I. Data on signal strenghts of $H \rightarrow \gamma\gamma$ recorded by ATLAS and CMS, and at the Tevatron *before* and *after* Moriond 2013. The luminosity updates at 8 TeV are shown in the parenthesis. The percentages of each production mode in each data are given (details are given in the text). The χ^2 of each data with respect to the SM is shown in the last two columns for *before* and *after* Moriond. The sub-totals χ^2 of this decay mode are shown at the end.

Channel	Signal strength μ		$M_H(\text{GeV})$	Production mode				$\chi^2_{\text{SM}}(\text{each})$	
	<i>Before</i>	<i>After</i>		ggF	VBF	VH	ttH	<i>Before</i>	<i>After</i>
ATLAS (4.8fb^{-1} at 7TeV + 13.0 (20.7) fb^{-1} at 8TeV): [9, 25]									
$\mu_{ggH+ttH}$	1.8 ± 0.49	1.6 ± 0.4	126.8	100%	-	-	-	2.67	2.25
μ_{VBF}	2.0 ± 1.4	1.7 ± 0.9	126.8	-	100%	-	-	0.53	0.60
μ_{VH}	1.9 ± 2.6	$1.8^{+1.5}_{-1.3}$	126.8	-	-	100%	-	0.12	0.38
CMS (5.1fb^{-1} at 7TeV + 5.3 (19.6) fb^{-1} at 8TeV) [13, 27]									
untagged	$1.42^{+0.55}_{-0.49}$	$0.78^{+0.28}_{-0.26}$	125	87.5%	7.1%	4.9%	0.5%	0.73	0.62
VBF tagged	$2.25^{+1.34}_{-1.04}$	$2.25^{+1.34}_{-1.04}$	125.8	17%	83%	-	-	1.44	1.44
Tevatron (10.0fb^{-1} at 1.96TeV): [7]									
Combined	$6.14^{+3.25}_{-3.19}$	$6.14^{+3.25}_{-3.19}$	125	78%	5%	17%	-	2.60	2.60
							subtot:	8.09	7.89

TABLE II. The same as Table I but for $H \rightarrow ZZ^{(*)}$.

Channel	Signal strength μ		$M_H(\text{GeV})$	Production mode				$\chi_{\text{SM}}^2(\text{each})$	
	<i>Before</i>	<i>After</i>		ggF	VBF	VH	ttH	<i>Before</i>	<i>After</i>
ATLAS (4.8fb^{-1} at 7TeV + 13 (20.7) fb^{-1} at 8TeV) [10, 26]									
Inclusive	1.0 ± 0.4	1.5 ± 0.4	125.5	87.5%	7.1%	4.9%	0.5%	0.0	1.56
CMS (5.1fb^{-1} at 7TeV + 12.2 (19.6) fb^{-1} at 8TeV) [14, 28]									
Inclusive	$0.80^{+0.35}_{-0.28}$	$0.91^{+0.30}_{-0.24}$	125.8	87.5%	7.1%	4.9%	0.5%	0.33	0.09
subtot:								0.33	1.65

 TABLE III. The same as Table I but for $H \rightarrow WW^{(*)}$.

Channel	Signal strength μ		$M_H(\text{GeV})$	Production mode				$\chi_{\text{SM}}^2(\text{each})$	
	<i>Before</i>	<i>After</i>		ggF	VBF	VH	ttH	<i>Before</i>	<i>After</i>
ATLAS (4.8fb^{-1} at 7TeV + 13 (20.7) fb^{-1} at 8TeV) [10, 26]									
Inclusive	1.5 ± 0.6	1.0 ± 0.3	125.5	87.5%	7.1%	4.9%	0.5%	0.69	0.00
CMS (up to 4.9fb^{-1} at 7TeV + 12.1 (19.5) fb^{-1} at 8TeV) [13, 29]									
0/1 jet	$0.77^{+0.27}_{-0.25}$	0.76 ± 0.21	125	97%	3%	-	-	0.73	1.31
VBF tag	$-0.05^{+0.74}_{-0.55}$	$-0.05^{+0.74}_{-0.55}$	125.8	17%	83%	-	-	2.01	2.01
VH tag	$-0.31^{+2.22}_{-1.94}$	$-0.31^{+2.22}_{-1.94}$	125.8	-	-	100%	-	0.35	0.35
Tevatron (10.0fb^{-1} at 1.96TeV): [7]									
Combined	$0.85^{+0.88}_{-0.81}$	$0.85^{+0.88}_{-0.81}$	125	78%	5%	17%	-	0.03	0.03
subtot:								3.81	3.70

TABLE IV. The same as Table I but for $H \rightarrow b\bar{b}$. There are no updates for this channel.

Channel	Signal strength μ		$M_H(\text{GeV})$	Production mode				$\chi_{\text{SM}}^2(\text{each})$	
	<i>Before</i>	<i>After</i>		ggF	VBF	VH	ttH	<i>Before</i>	<i>After</i>
ATLAS (4.8fb^{-1} at 7TeV + 13.0fb^{-1} at 8TeV) [26]									
VH tag	-0.4 ± 1.0		125.5	-	-	100%	-		1.96
CMS (up to 5.0fb^{-1} at 7TeV + 12.1fb^{-1} at 8TeV) [13]									
VH tag	$1.31^{+0.65}_{-0.60}$		125.8	-	-	100%	-		0.27
ttH tag	$-0.80^{+2.10}_{-1.84}$		125.8	-	-	-	100%		0.73
Tevatron (10.0fb^{-1} at 1.96TeV): [8]									
VH tag	$1.56^{+0.72}_{-0.73}$		125	-	-	100%	-		0.59
								subtot:	3.55

TABLE V. The same as Table I but for $H \rightarrow \tau\tau$. The correlation for the $\tau\tau$ data of ATLAS is $\rho = -0.50$ and -0.49 before and after Moriond, respectively. The percentages of the production modes differ very tiny before and after Moriond.

Channel	Signal strength μ		$M_H(\text{GeV})$	Production mode				$\chi_{\text{SM}}^2(\text{each})$	
	<i>Before</i>	<i>After</i>		ggF	VBF	VH	ttH	<i>Before</i>	<i>After</i>
ATLAS (4.6fb^{-1} at 7TeV + 13.0fb^{-1} at 8TeV) [11, 26]									
$\mu(ggF)$	2.38 ± 1.57	2.30 ± 1.60	125.5	100%	-	-	-	1.60	1.41
$\mu(VBF + VH)$	-0.25 ± 1.02	-0.22 ± 1.06	125.5	-	59.4%	40.6%	-		
CMS (up to 4.9fb^{-1} at 7TeV + $12.1 (19.4)\text{fb}^{-1}$ at 8TeV) [13, 30]									
0/1 jet	$0.85^{+0.68}_{-0.66}$	$0.76^{+0.50}_{-0.52}$	125	77.8%	13.8%	7.6%	0.8%	0.05	0.23
VBF tag	$0.82^{+0.82}_{-0.75}$	$1.40^{+0.59}_{-0.57}$	125	20.9%	79.1%	-	-	0.05	0.49
VH tag	$0.86^{+1.92}_{-1.68}$	$0.77^{+1.49}_{-1.42}$	125	-	-	100%	-	0.005	0.02
								subtot:	1.70 2.15

TABLE VI. The best fitted values and the 1σ errors for the parameters in various CP conserving fits and the corresponding chi-square per degree of freedom and the p -value before and after the Moriond 2013. The p -values for the SM fit are 0.74 and 0.65 for the data before and after the Moriond, respectively.

Parameters	Vary $\Delta\Gamma_{\text{tot}}$	Vary ΔS^γ , ΔS^g	Vary ΔS^γ , $\Delta S^g, \Delta\Gamma_{\text{tot}}$	Vary C_u^S, C_d^S , C_ℓ^S, C_v	Vary $C_u^S, C_d^S, C_\ell^S, C_v$ $\Delta S^\gamma, \Delta S^g$
	Before Moriond				
C_u^S	1	1	1	$-0.88^{+0.16}_{-0.21}$	0.00 ± 1.13
C_d^S	1	1	1	$1.12^{+0.45}_{-0.38}$	$1.19^{+0.57}_{-0.41}$
C_ℓ^S	1	1	1	$-0.97^{+0.30}_{-0.29}$	0.98 ± 0.30
C_v	1	1	1	$0.97^{+0.13}_{-0.15}$	$0.96^{+0.13}_{-0.15}$
ΔS^γ	0	$-2.73^{+1.11}_{-1.15}$	$-2.93^{+1.19}_{-1.31}$	0	$-1.23^{+2.44}_{-2.49}$
ΔS^g	0	$-0.050^{+0.064}_{-0.065}$	$0.0063^{+0.15}_{-0.11}$	0	$0.73^{+0.81}_{-0.80}$
$\Delta\Gamma_{\text{tot}}$ (MeV)	$-0.022^{+0.63}_{-0.48}$	0	$0.79^{+2.01}_{-1.11}$	0	0
χ^2/dof	17.48/21	11.27/20	10.83/19	10.46/18	9.89/16
p -value	0.68	0.94	0.93	0.92	0.87
After Moriond					
C_u^S	1	1	1	$0.80^{+0.16}_{-0.13}$	0.00 ± 1.18
C_d^S	1	1	1	$-0.98^{+0.31}_{-0.34}$	$1.06^{+0.41}_{-0.35}$
C_ℓ^S	1	1	1	$0.98^{+0.21}_{-0.21}$	1.01 ± 0.23
C_v	1	1	1	$1.04^{+0.12}_{-0.14}$	$1.01^{+0.13}_{-0.14}$
ΔS^γ	0	$-0.96^{+0.84}_{-0.85}$	$-0.96^{+0.84}_{-0.87}$	0	$0.78^{+2.34}_{-2.28}$
ΔS^g	0	-0.043 ± 0.052	$-0.040^{+0.12}_{-0.086}$	0	$0.66^{+0.42}_{-0.83}$
$\Delta\Gamma_{\text{tot}}$ (MeV)	$0.10^{+0.51}_{-0.41}$	0	$0.027^{+1.33}_{-0.80}$	0	0
χ^2/dof	18.89/21	17.55/20	17.55/19	17.82/18	16.89/16
p -value	0.59	0.62	0.55	0.48	0.39

TABLE VII. The best fitted values and the 1σ errors for the parameters in the CP-violating fits and the corresponding chi-square before and after Moriond 2013.

Parameters	Vary $\Delta S^\gamma, \Delta S^g, \Delta P^\gamma, \Delta P^g$		Vary C_u^S, C_u^P, C_v	
Before Moriond				
C_u^S	1	1	$-0.54^{+0.65}_{-0.39}$	$-0.54^{+0.65}_{-0.39}$
C_d^S	1	1	1	1
C_ℓ^S	1	1	1	1
C_v	1	1	$0.93^{+0.10}_{-0.12}$	$0.93^{+0.10}_{-0.12}$
ΔS^γ	$0.28^{+16.9}_{-4.16}$	$-0.28^{+17.4}_{-3.60}$	0	0
ΔS^g	$-0.62^{+0.63}_{-0.70}$	$-0.62^{+0.63}_{-0.70}$	0	0
$\Delta\Gamma_{\text{tot}}$ (MeV)	0	0	0	0
C_u^P	0	0	$-0.46^{+1.14}_{-0.22}$	$0.46^{+1.14}_{-0.22}$
ΔP^γ	$-6.88^{+17.4}_{-3.64}$	$-6.31^{+16.8}_{-4.21}$	0	0
ΔP^g	$0.60^{+0.065}_{-1.26}$	$0.60^{+0.065}_{-1.26}$	0	0
χ^2/dof	11.26/18	11.26/18	10.53/19	10.53/19
p -value	0.88	0.88	0.94	0.94
After Moriond				
C_u^S	1	1	$0.48^{+0.44}_{-0.48}$	$0.48^{+0.44}_{-0.48}$
C_d^S	1	1	1	1
C_ℓ^S	1	1	1	1
C_v	1	1	$0.995^{+0.097}_{-0.104}$	$0.995^{+0.097}_{-0.104}$
ΔS^γ	$-0.92^{+16.00}_{-0.89}$	$0.71^{+14.37}_{-2.51}$	0	0
ΔS^g	$-0.55^{+0.56}_{-0.76}$	$-0.64^{+0.65}_{-0.67}$	0	0
$\Delta\Gamma_{\text{tot}}$ (MeV)	0	0	0	0
C_u^P	0	0	$0.50^{+0.11}_{-0.40}$	$-0.50^{+0.44}_{-0.11}$
ΔP^γ	$0.77^{+7.67}_{-9.21}$	$4.75^{+3.69}_{-13.19}$	0	0
ΔP^g	$-0.60^{+1.26}_{-0.06}$	$-0.61^{+1.27}_{-0.052}$	0	0
χ^2/dof	17.55/18	17.55/18	17.17/19	17.17/19
p -value	0.49	0.49	0.58	0.58

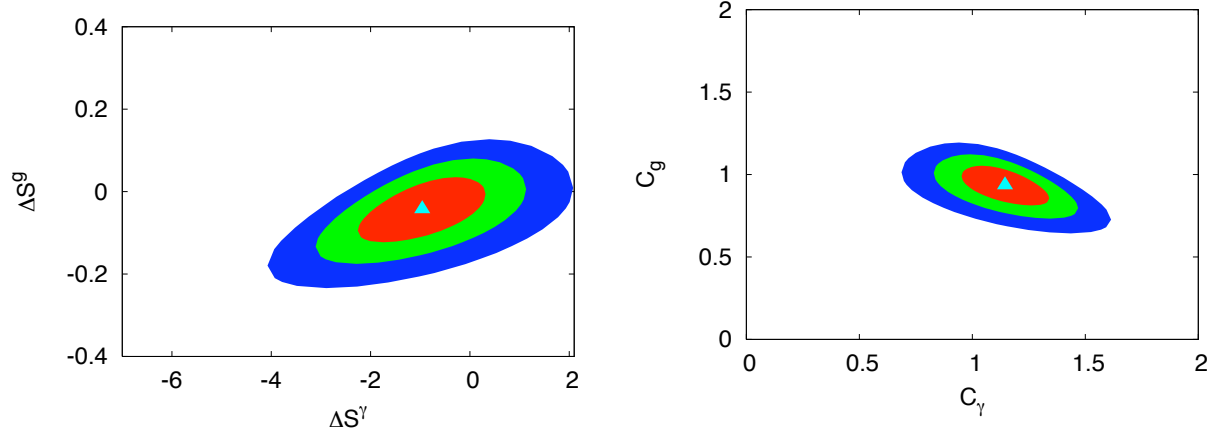


FIG. 1. The confidence-level regions of the fit by varying ΔS^γ and ΔS^g only, (a) in the $(\Delta S^\gamma, \Delta S^g)$ plane and (b) in the corresponding (C_γ, C_g) plane. The contour regions shown are for $\Delta\chi^2 \leq 2.3$ (red), 5.99 (green), and 11.83 (blue) above the minimum, which correspond to confidence levels of 68.3%, 95%, and 99.7%, respectively. The best-fit point is denoted by the triangle.

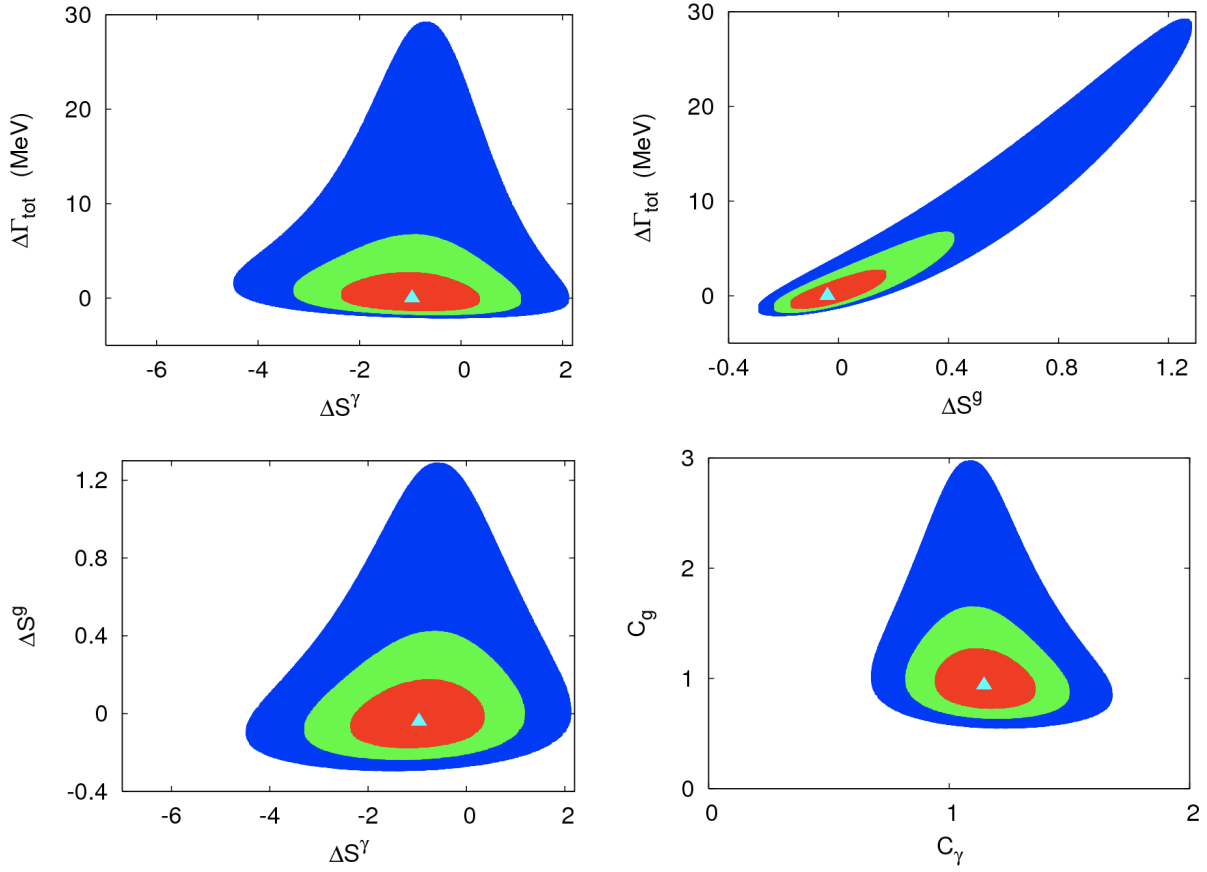


FIG. 2. The confidence-level regions of the fit by varying ΔS^γ , ΔS^g , and $\Delta\Gamma_{\text{tot}}$, (a) in the $(\Delta S^\gamma, \Delta\Gamma_{\text{tot}})$ plane, (b) in the $(\Delta S^g, \Delta\Gamma_{\text{tot}})$ plane, (c) in the $(\Delta S^\gamma, \Delta S^g)$ plane, (d) in the corresponding (C_γ, C_g) plane. The description of contour regions is the same as Fig. 1.

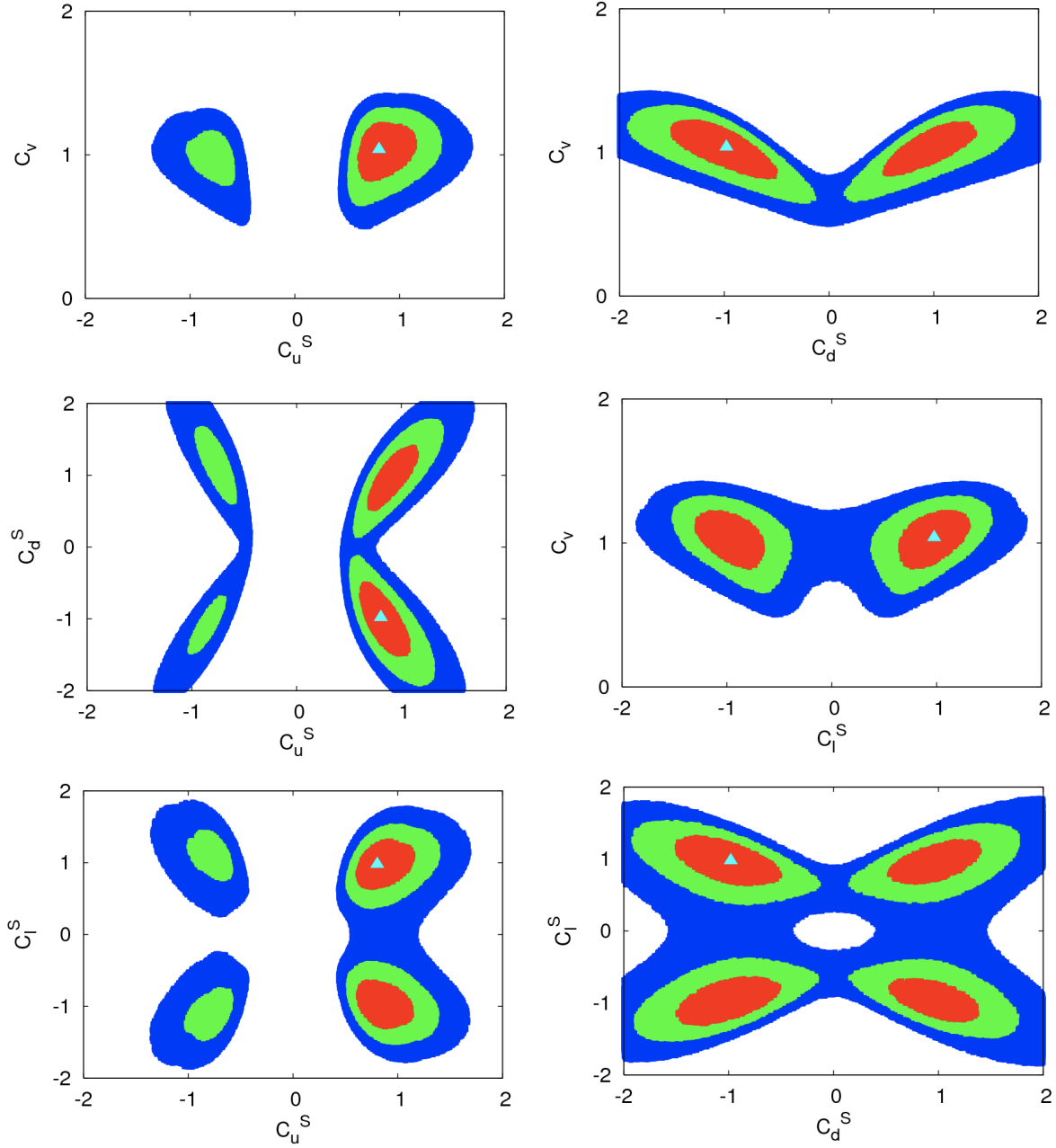


FIG. 3. The confidence-level regions of the fit by varying C_u^S , C_d^S , C_l^S and C_v while keeping $\Delta S^\gamma = \Delta S^g = \Delta \Gamma_{\text{tot}} = 0$. The description of contour regions is the same as Fig. 1.

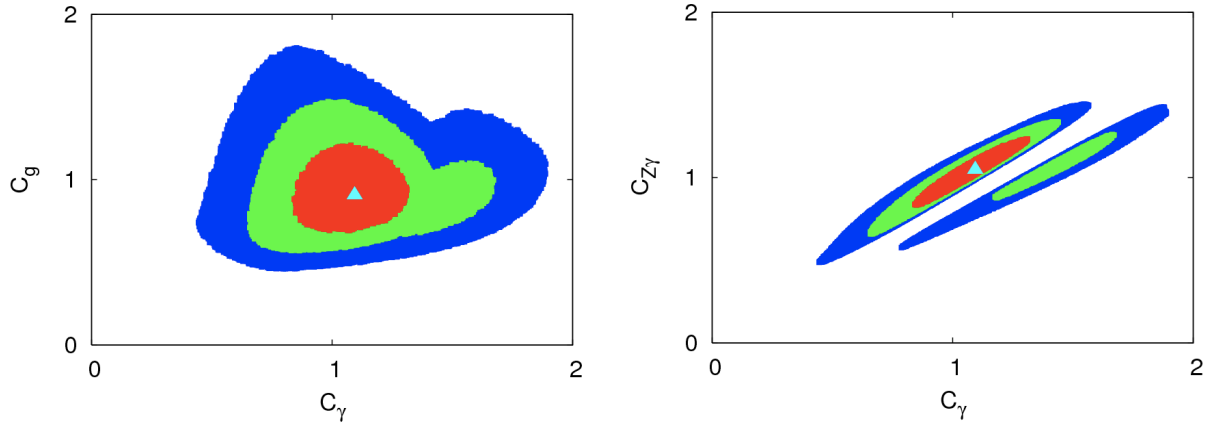


FIG. 4. (a) Same as Fig. 3 but in the corresponding plane of (C_γ, C_g) . (b) Prediction in the corresponding $(C_\gamma, C_{Z\gamma})$ plane. The description of contour regions is the same as Fig. 1.

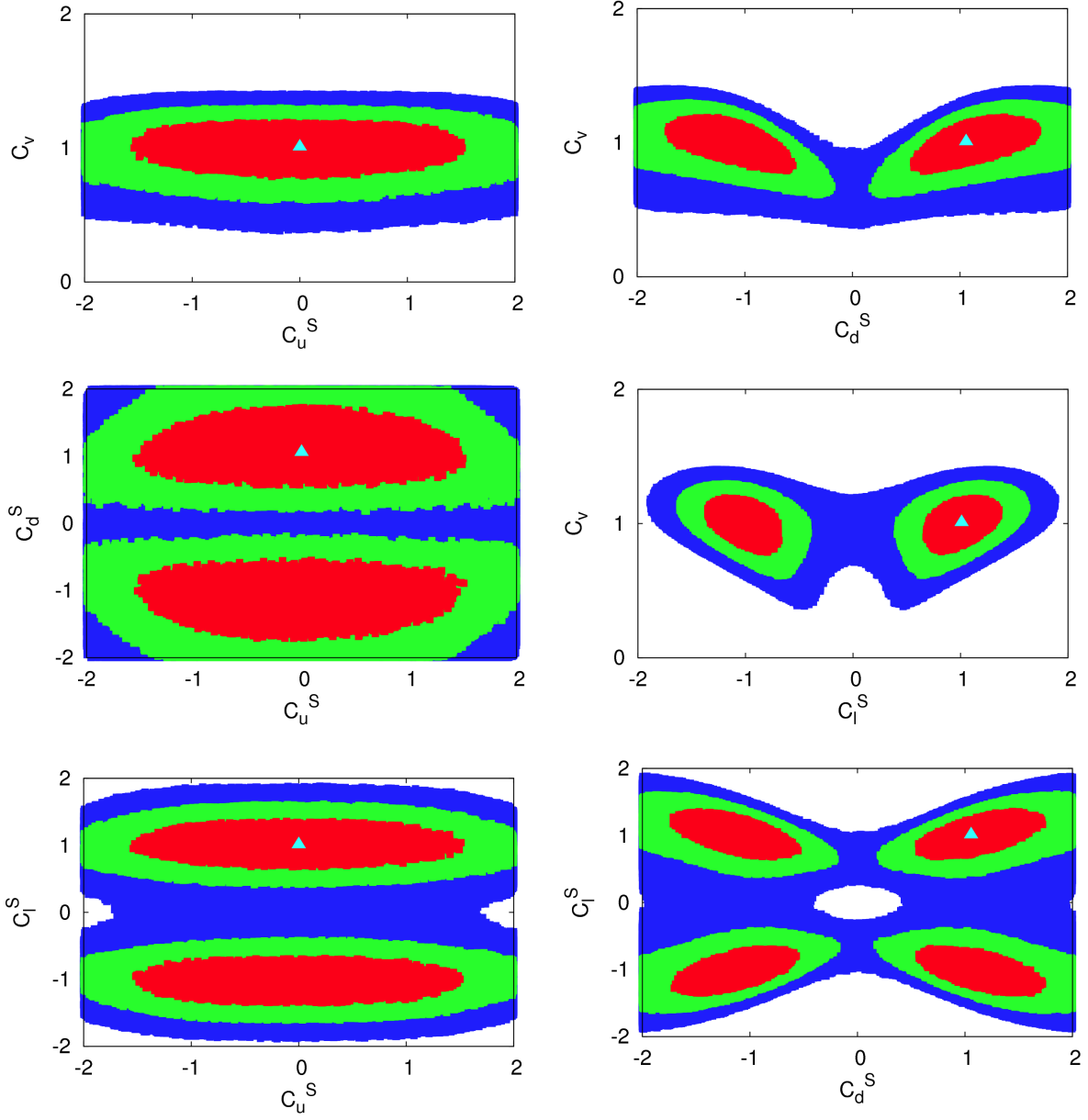


FIG. 5. The confidence-level regions of the fit by varying C_u^S , C_d^S , C_l^S , C_v , ΔS^γ and ΔS^g while keeping $\Delta\Gamma_{\text{tot}} = 0$. Shown are the correlations among $(C_u^S, C_d^S, C_l^S, C_v)$. The description of contour regions is the same as Fig. 1.

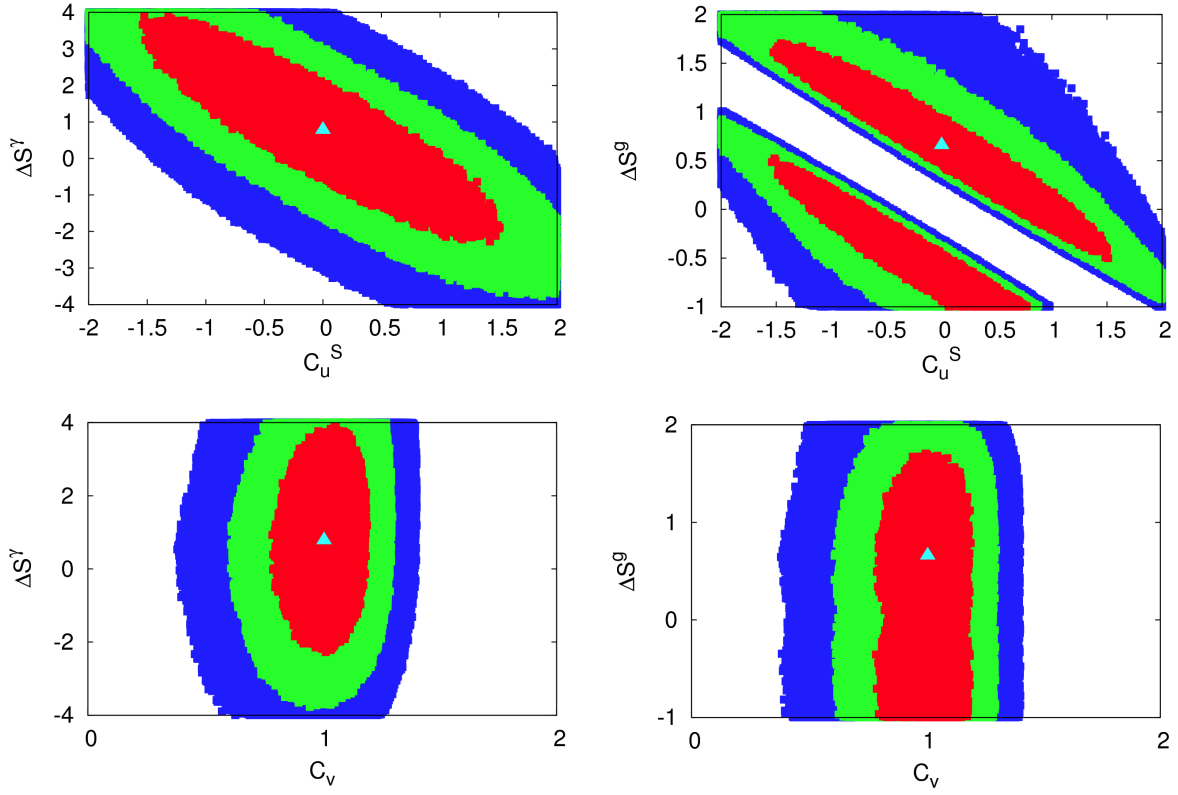


FIG. 6. Same as Fig. 5. Shown are the correlations between (C_u^S, C_v) and $(\Delta S^\gamma, \Delta S^g)$.

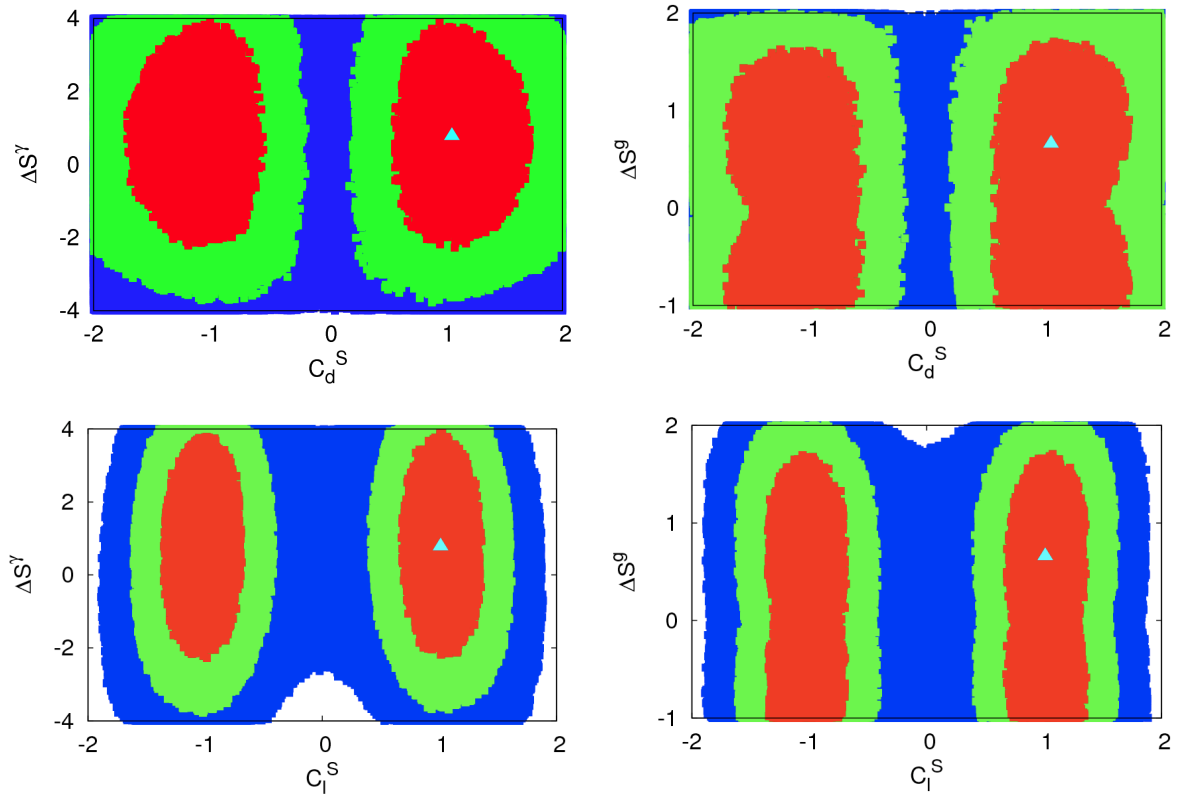


FIG. 7. Same as Fig. 5. Shown are the correlations between (C_d^S, C_l^S) and $(\Delta S^\gamma, \Delta S^g)$.

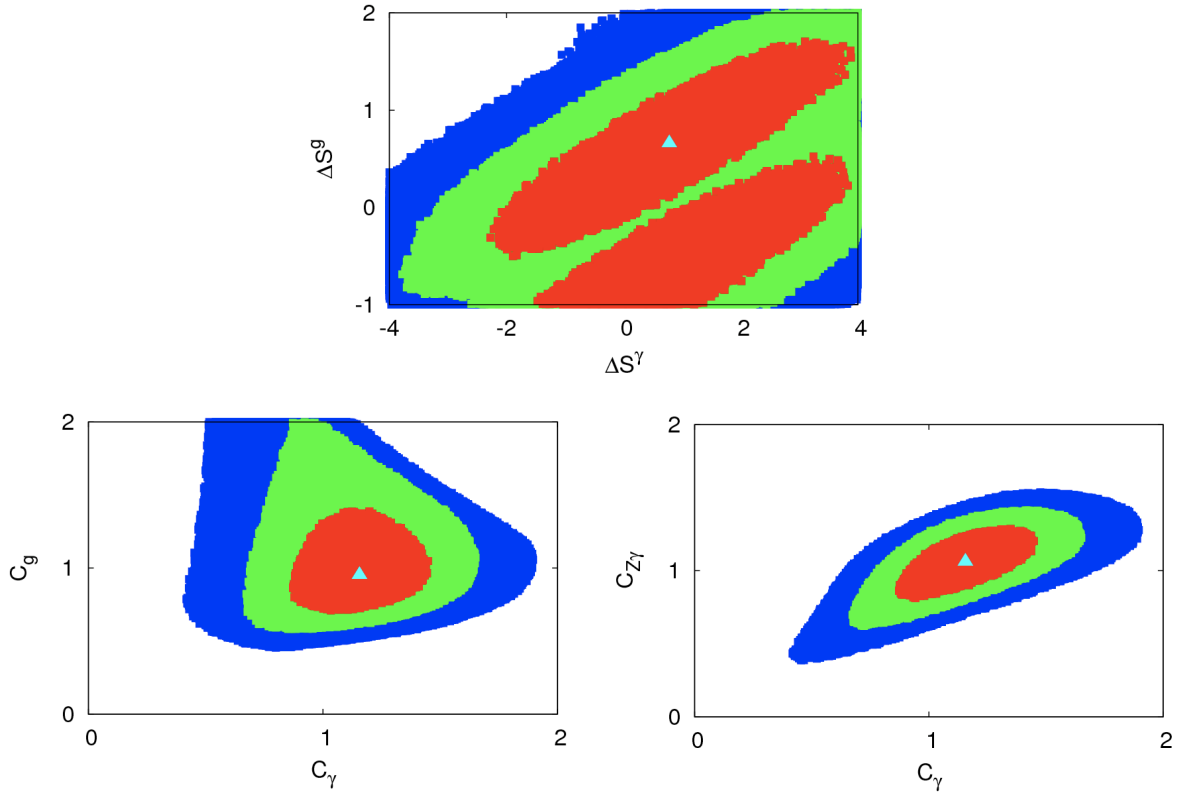


FIG. 8. Same as Fig. 5. Shown are the correlations between ΔS^γ and ΔS^g , between C_γ and C_g , and between C_γ and $C_{Z\gamma}$.

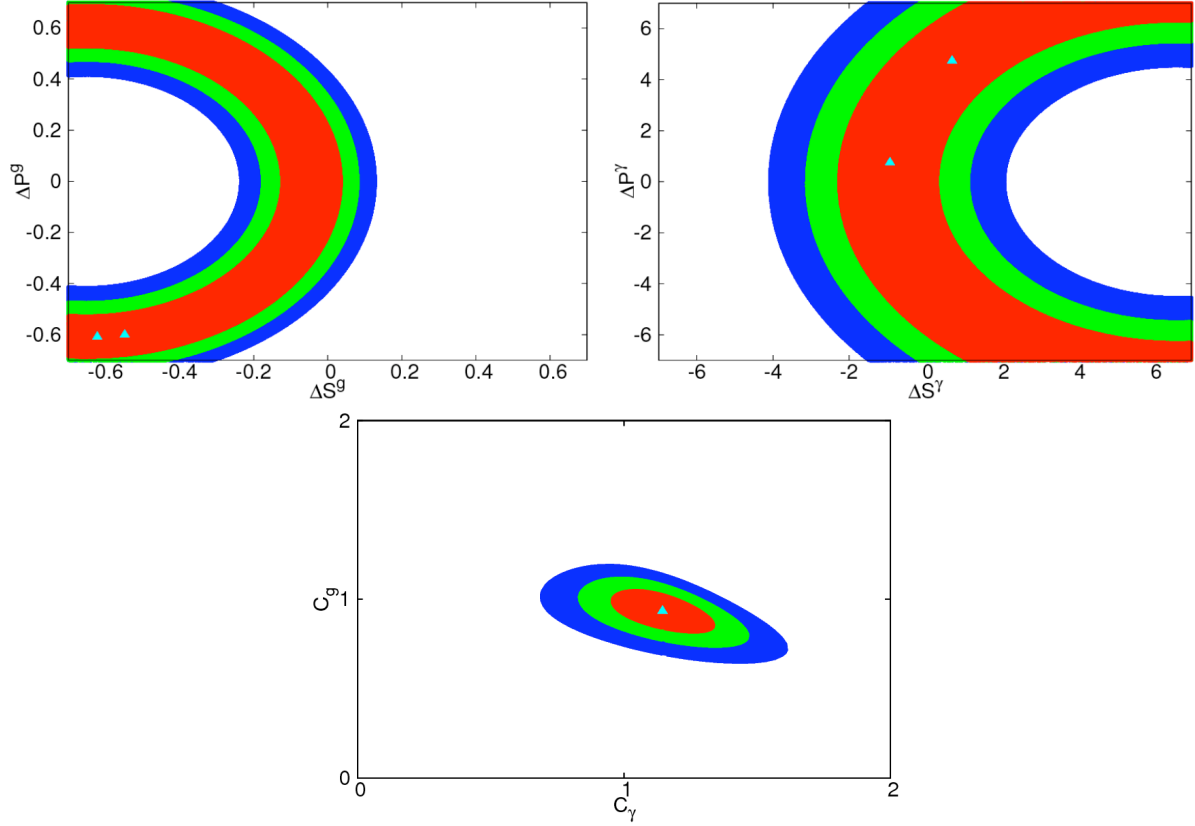


FIG. 9. The confidence-level regions of the fit by varying the scalar contributions ΔS^γ and ΔS^g , and the pseudoscalar contributions ΔP^γ and ΔP^g while keeping $C_u^S = C_d^S = C_\ell^S = 1$, $C_u^P = C_d^P = C_\ell^P = 0$ and $\Delta\Gamma_{\text{tot}} = 0$. The description of contour regions is the same as Fig. 1.

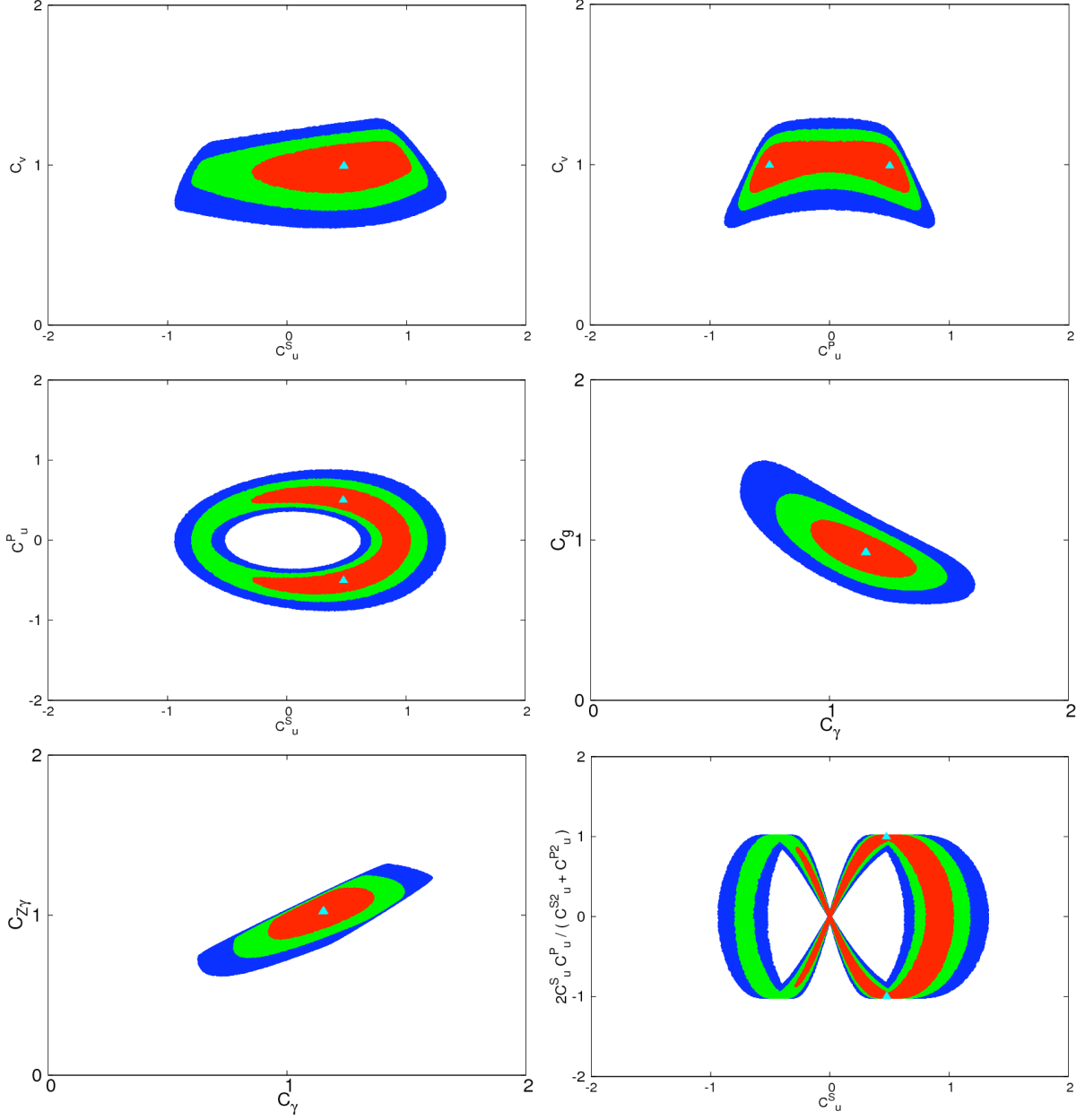


FIG. 10. The confidence-level regions of the fit by varying the scalar Yukawa couplings C_u^S and C_v , and the pseudoscalar Yukawa couplings C_u^P ; while keeping $C_d^S = C_\ell^S = 1$, $C_d^P = C_\ell^P = 0$, and $\Delta S^\gamma = \Delta S^g = \Delta P^\gamma = \Delta P^g = \Delta\Gamma_{\text{tot}} = 0$. The description of contour regions is the same as Fig. 1.

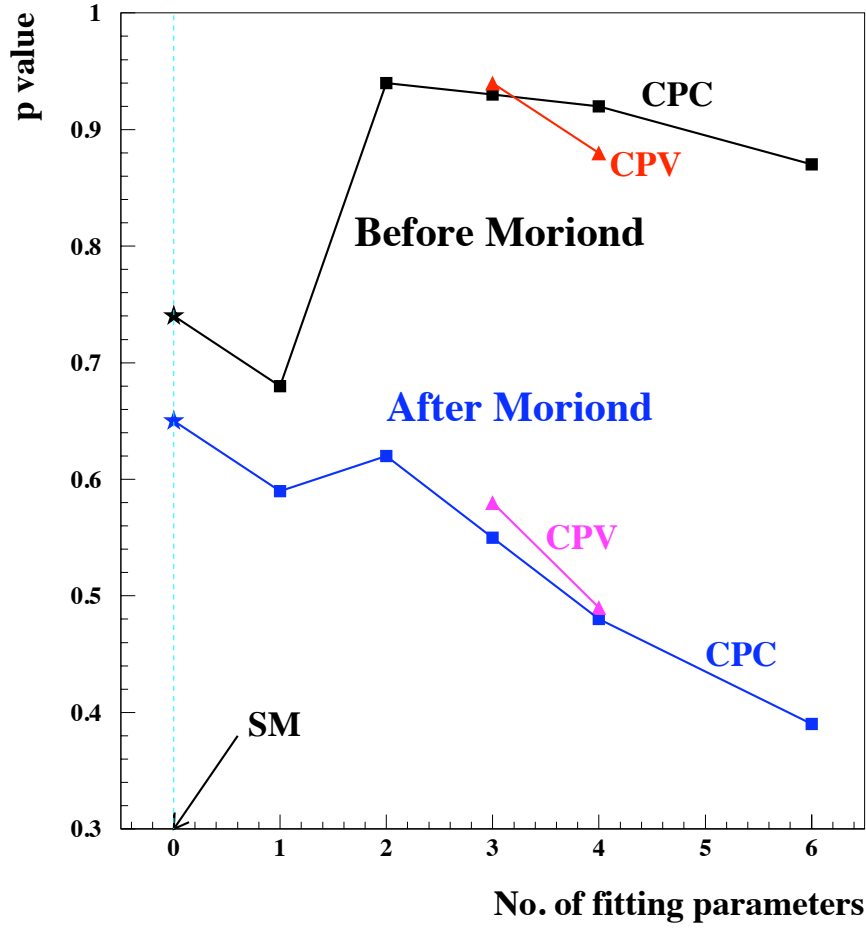


FIG. 11. The p -values for various fits considered in this work, including CP-conserving (CPC) and CP-violating (CPV) ones. The CPC cases with the No. of fitting parameters equals 1 denotes the case varying only $\Delta\Gamma_{\text{tot}}$; 2 denotes varying only ΔS^γ and ΔS^g ; 3 denotes varying only ΔS^γ , ΔS^g , and $\Delta\Gamma_{\text{tot}}$; 4 denotes varying only C_u^S , C_d^S , C_ℓ^S , and C_v ; 6 denotes varying C_u^S , C_d^S , C_ℓ^S , C_v , ΔS^γ , and ΔS^g . The CPV cases with the No. of fitting parameters equals 3 denotes varying only C_u^S , C_u^P , and C_v ; 4 denotes varying only ΔS^γ , ΔS^g , ΔP^γ , and ΔP^g .